SPACE TELESCOPE MOMENTUM

MANAGEMENT PROCEDURES

(REVISION 2)

Prepared for

GODDARD SPACE FLIGHT CENTER

By

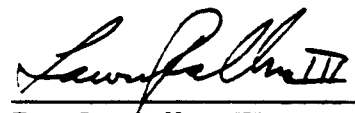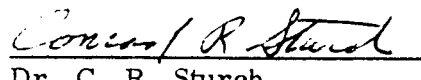COMPUTER SCIENCES CORPORATION
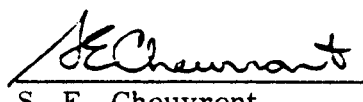
Under

Contract NAS 5-24300
Task Assignment 14500

Prepared by:

Approved by:

Dr. L. C. Chen   Date
General Software Corporation

Dr. L. Fallon III   Date
Section Manager

Dr. C. R. Sturch   Date
Task Leader

S. E. Cheuvront   Date
Department Manager

ABSTRACT

This technical.memorandum presents an analysis of the minimum energy and cross product momentum management control laws which have been selected for use in the Space Telescope mission. The ground support requirements for implementation of the minimum energy law are discussed. The impact of each law on routine operations and the scientific program is assessed. This document also includes physical interpretations of control laws, suggestions for new procedures, and discussion of published accuracy requirements for the implementation of the original control laws. This revised version of the document contains corrections of minor errors in the earlier versions and a more detailed presentation of the implementation of the minimum energy law during maneuvers.

TABLE OF CONTENTS

TABLE OF CONTENTS (Cont'd)

LIST OF ILLUSTRATIONS

LIST OF TABLES

SECTION 1 - INTRODUCTION

The Space Telescope (ST) is an astronomical observatory to be launched in late 1983 or early 1984 by the Space Shuttle into a nominal 500-kilometer circular orbit. The Pointing Control System (PCS) provides the attitude reference and control stability for the ST. The most challenging requirement of the PCS is the pointing stability of 0.007 arc-second (one sigma) (Reference 1-1).

The PCS uses software residing in the onboard flight computer and hardware located throughout the Support Systems Module (SSM) to accomplish these goals. Major hardware components used by the PCS are shown in Figure 1-1. The Sun sensors and fixed-head star trackers are required primarily for initial attitude determination and recovery. Each of the three fine guidance sensors (FGSs) track star images within a quadrant of the telescope focal surface extending from 10.2 to 14 arc-minutes off the optical (+V1) axis (Reference 1-2). The output of two FGSs is used by the PCS for position error and rate determination. Additional rate information is provided by the three rate gyro assemblies (RGAs) that contain a total of six gyros, four of which are used for nominal operation. The PCS actuates torques through four reaction wheel assemblies (RWAs) mounted in a skewed configuration. Excess speed is removed from the reaction wheels by a set of four magnetic torquer (MT) bars that interact with the Earth's magnetic field. The torque generated by the MTs is applied directly to the SSM body and then transferred to the reaction wheels. The configurations of the RWAs and MTs are shown in Figures 1-2 and and 1-3, respectively. Measurements of the geomagnetic field are provided to the PCS by two redundant three-axis magnetometers.

The PCS uses the Digital 224 Flight Computer to process input from the Sun sensors, fixed-head star trackers, FGSs, RGAs, and magnetometers and to command the MTs and RWAs. Figure 1-4 is a block diagram of the PCS. This document is primarily concerned with operational and scientific impacts
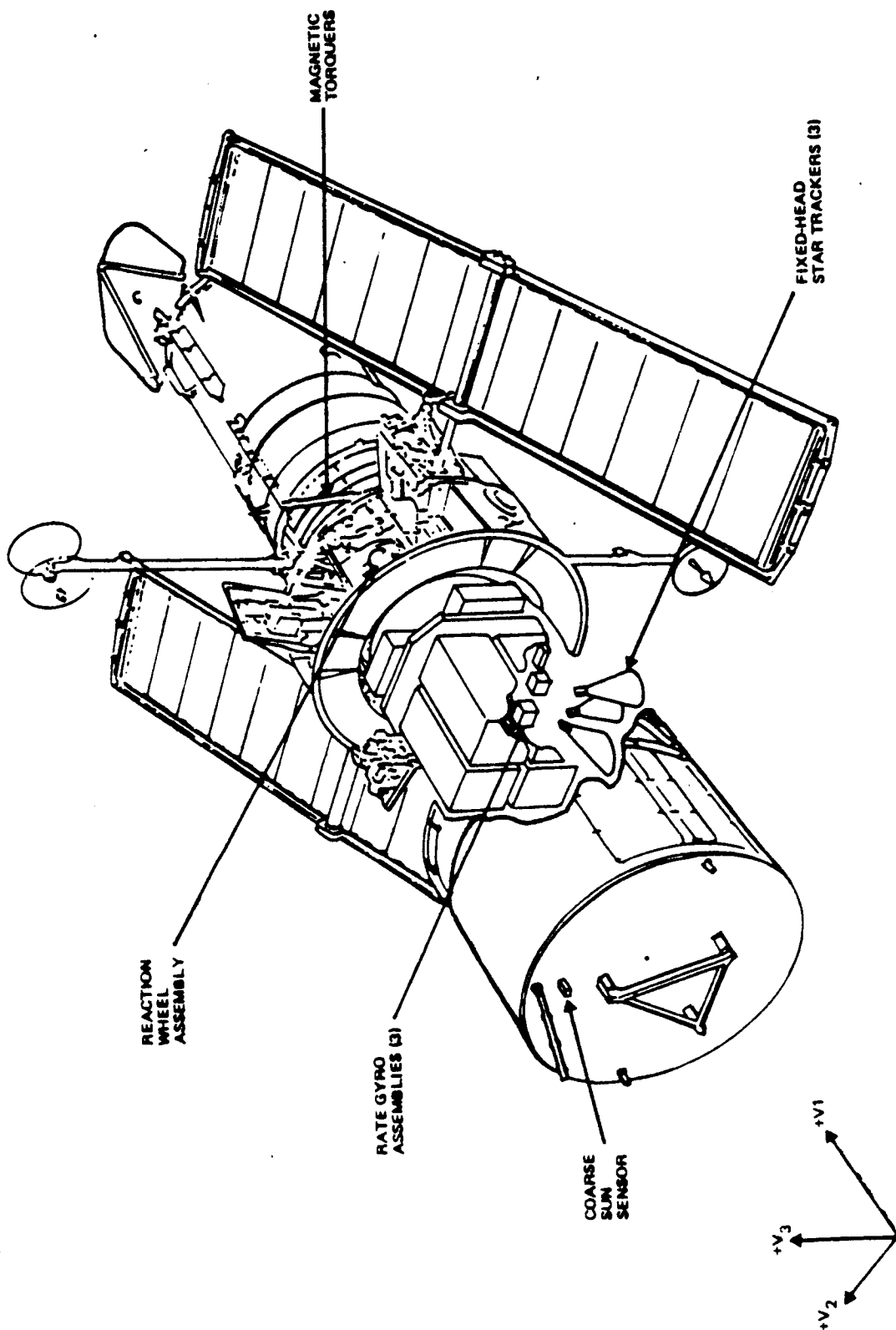
Figure 1-1. Major PCS Hardware Items. (The figure is adapted from Reference 1-1.)

NO. 3 (IN FRONT)
NO. 4 (BEHIND)

NO. 1 (IN FRONT)
NO. 2 (BEHIND)

H_{RW3} H_{RW1}

45° 45°

A   A

V_2

V_1

H_{RW4} H_{RW3}

20° 20°
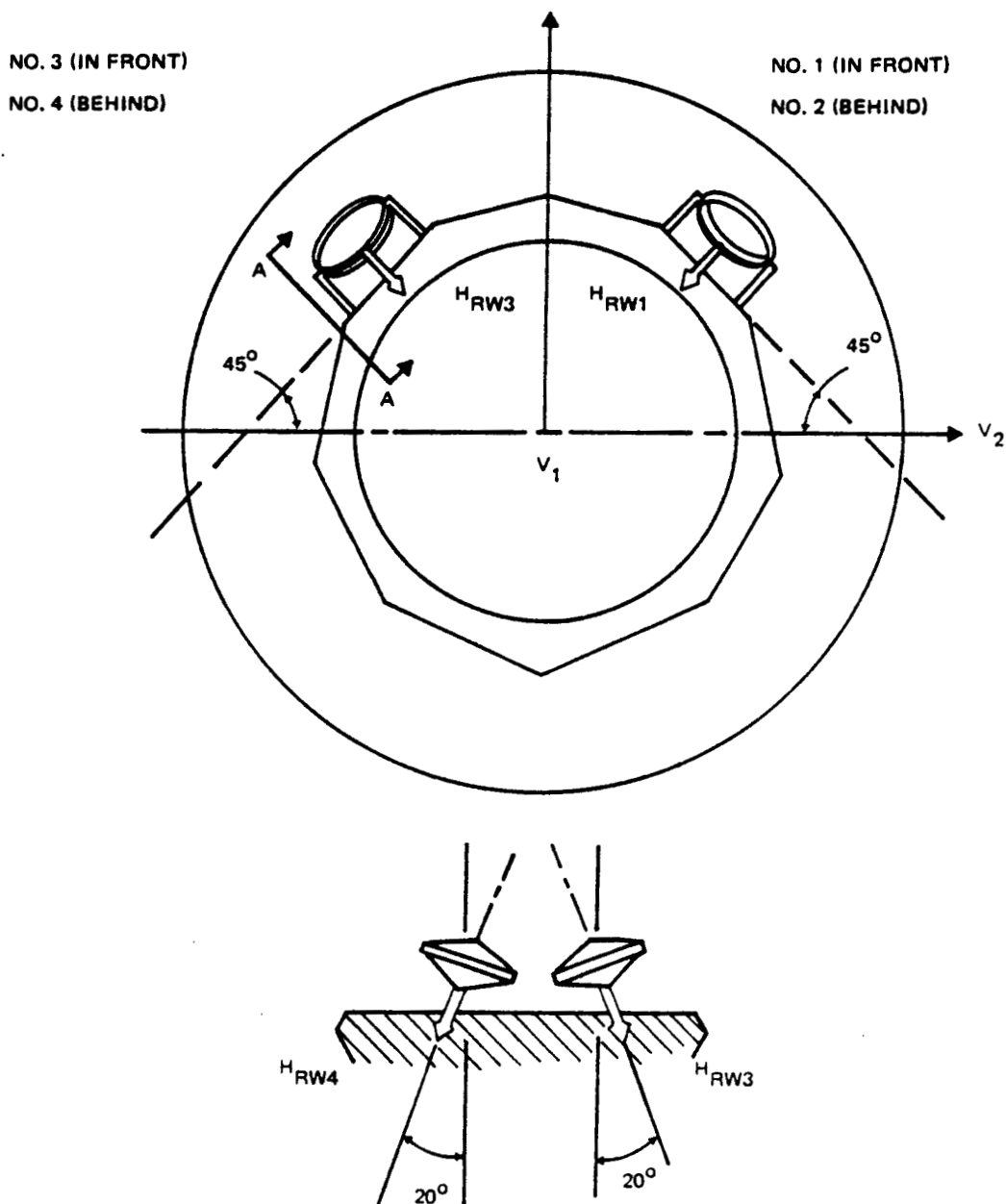
Figure 1-2. Reaction Wheel Configuration. (The figure is
adapted from Reference 1-2.)
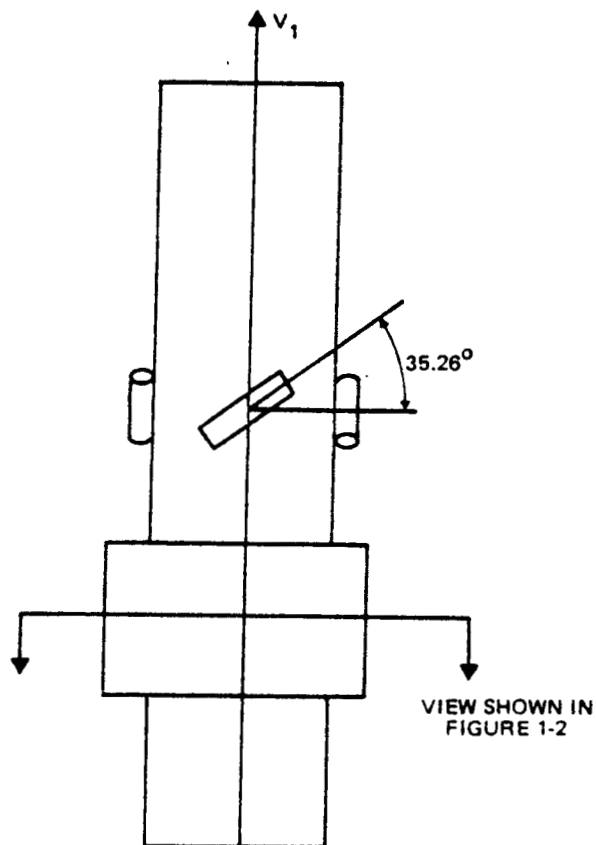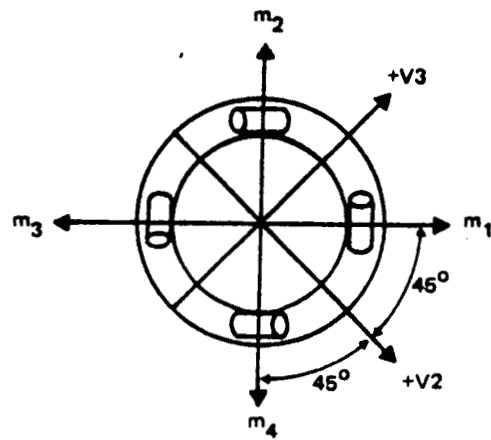
Figure 1-3. Magnetic Torquer Configuration. (The figure is adapted from Reference 1-2.)
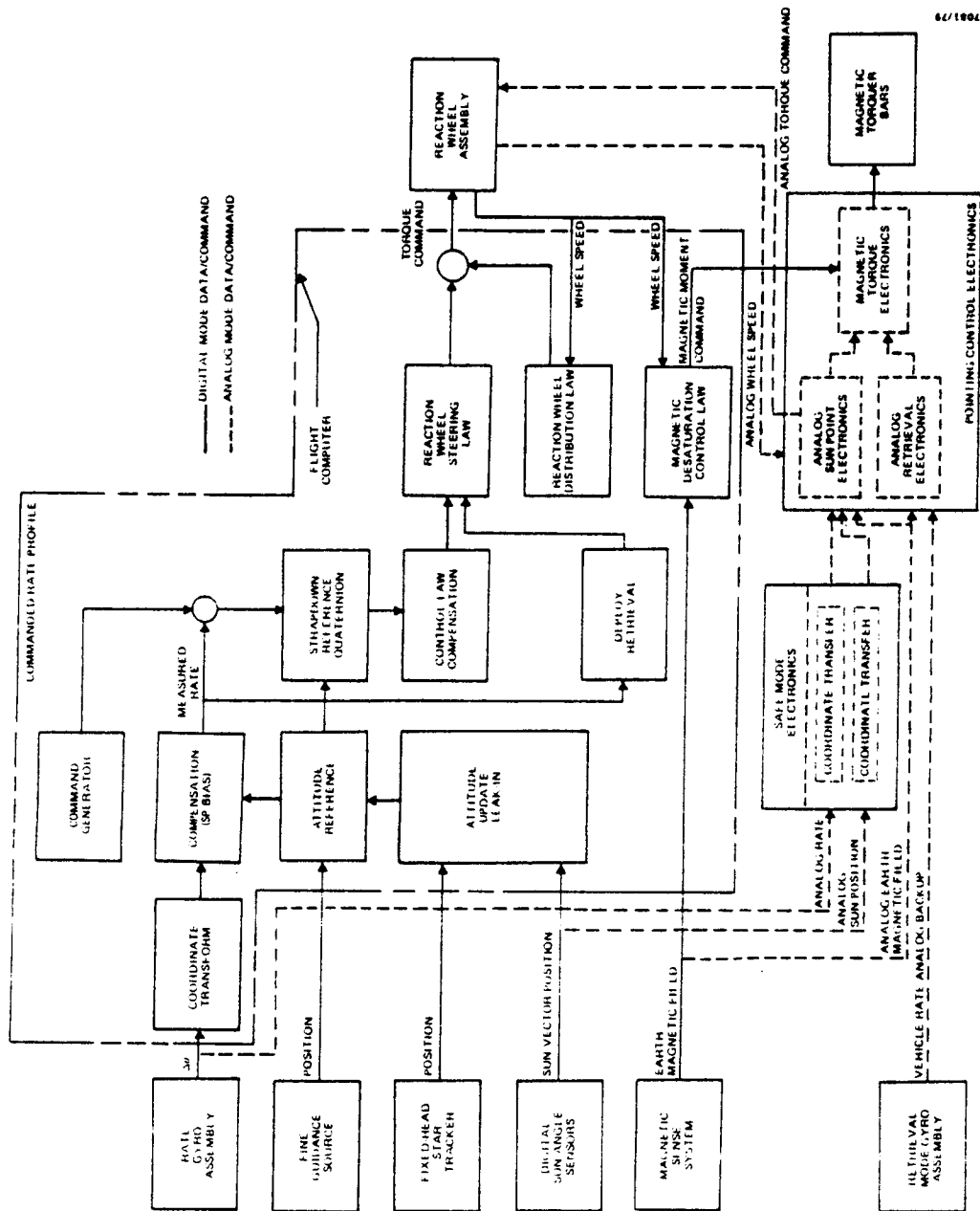
Figure 1-4. Pointing Control System. (The figure is adapted from Reference 1-1.)

1-5

of magnetic desaturation or momentum management control laws, i.e., the methods by which the commanded magnetic torques are computed for control of the reaction wheel speeds.

To achieve the 0.007-arc-second stability required in the fine pointing mode, vibrations generated by the rotating reaction wheels must not excite significant ST bending modes. Because the dominant vibration produced by the RWAs occurs at the rotational frequency of the reaction wheels, it is required that reaction wheel speeds remain below approximately 600 rpm (10 hertz) while the ST is in the fine pointing mode (References 1-2 through 1-4). The momentum management control is required to limit the reaction wheels to 10 hertz under normal operating conditions and also in the case of RWA or MT failure. It is also desired that the smallest possible magnetic dipole moments be employed to keep the magnetic contamination of the ST scientific instruments within acceptable levels.

Several momentum management control laws have been proposed for desaturating the reaction wheels (References 1-2 and 1-3), two of which are recommended by Lockheed Missiles and Space Company. These are the minimum energy (ME) control law and the cross product (CP) control law. The ME control law minimizes the amount of energy required to generate the control magnetic dipole over a given time interval, which will bring the SSM angular momentum to a desired final value. The CP law is a closed-loop law that computes a deterministic control magnetic dipole proportional to the error signal with the constraint that it always be perpendicular to the Earth's magnetic field. The CP law can be implemented entirely onboard the ST and must be used during initial phases of the mission and during safe mode operations when interface with the Space Telescope Operations Control Center (STOCC) is unreliable. The ME law requires significant ground support.

Section 2 presents an analysis of the CP and ME control laws, including derivations of the laws, descriptions of onboard implementation, and delineation

of the ground system support requirements. Section 3 contains an analytical study of computation required on the ground for implementation of the ME law. In Section 4, the impact of each law on routine operations and the scientific program is discussed. Estimates of resources required to support each law also are given in Section 4. Section 5 discusses the physical interpretation of control laws. This section describes control laws in general, summarizes the current control laws implemented for ST, and presents alternative techniques for both inertial targets and maneuvers. Section 6 delineates the mathematical models used in the current control laws implemented for ST and reviews the published accuracy requirements and estimates for these models.

REFERENCES

1-1.   Lockheed Missiles and Space Company, LMSC 4171847A, ST Mission Operations Requirements, DR OP-01, volume III, August 1979

1-2.   A. Wernli, "Minimization of Reaction Wheel Momentum Storage with Magnetic Torquers," J. Astronautical Sciences, vol. 26, no. 3, p. 257, July-September 1978

1-3.   Lockheed Missiles and Space Company, LMSC-HREC TM D496086, Reaction Wheel Speed Minimization through Magnetic Desaturation, A. Wernli, November 1976

1-4.   --, SE-03, Section H, Space Telescope Project, Support Systems Module, Appendix 3, April 1979

SECTION 2 – ANALYSIS OF ONBOARD MOMENTUM MANAGEMENT SCHEMES

2.1 GENERAL ANALYTICAL CONSIDERATIONS

This section provides some analytical considerations which apply in general to all momentum management desaturation control laws. Specific considerations for the cross product (CP) and minimum energy (ME) control laws are given in Sections 2.2 and 2.3, respectively.

The interaction of the desaturation law with the components of the ST is schematically shown in Figure 2-1 (adopted from Reference 2-1). For any given measured reaction wheel (RW) system angular momentum, $\vec{H}_{RW}$, the desaturation law computes the commanded magnetic dipole moment, $\vec{\mu}_T$, for the four magnetic torquers. The components of $\vec{\mu}_T$ then combine to form the system magnetic dipole moment vector, $\vec{\mu}_M$, through the following relation:

$$\vec{\mu}_M = \begin{bmatrix} s & s & s & s \\ c & -c & -c & c \\ c & c & -c & -c \end{bmatrix} \vec{\mu}_T = M\,\vec{\mu}_T \qquad (2-1)$$

where $s = \sin 35.26^{\circ}$

$c = (1/\sqrt{2})\cos 35.26^{\circ}$

The matrix M in Equation (2-1) is called the magnetic coil mounting matrix, which results from the magnetic torquer mounting configuration shown in Figure 1-3. The interaction between the system magnetic dipole moment $\vec{\mu}_M$ and the geomagnetic field $\vec{B}$ produces a magnetic torque given by

$$\vec{T}_M = \vec{\mu}_M \times \vec{B} \qquad (2-2)$$
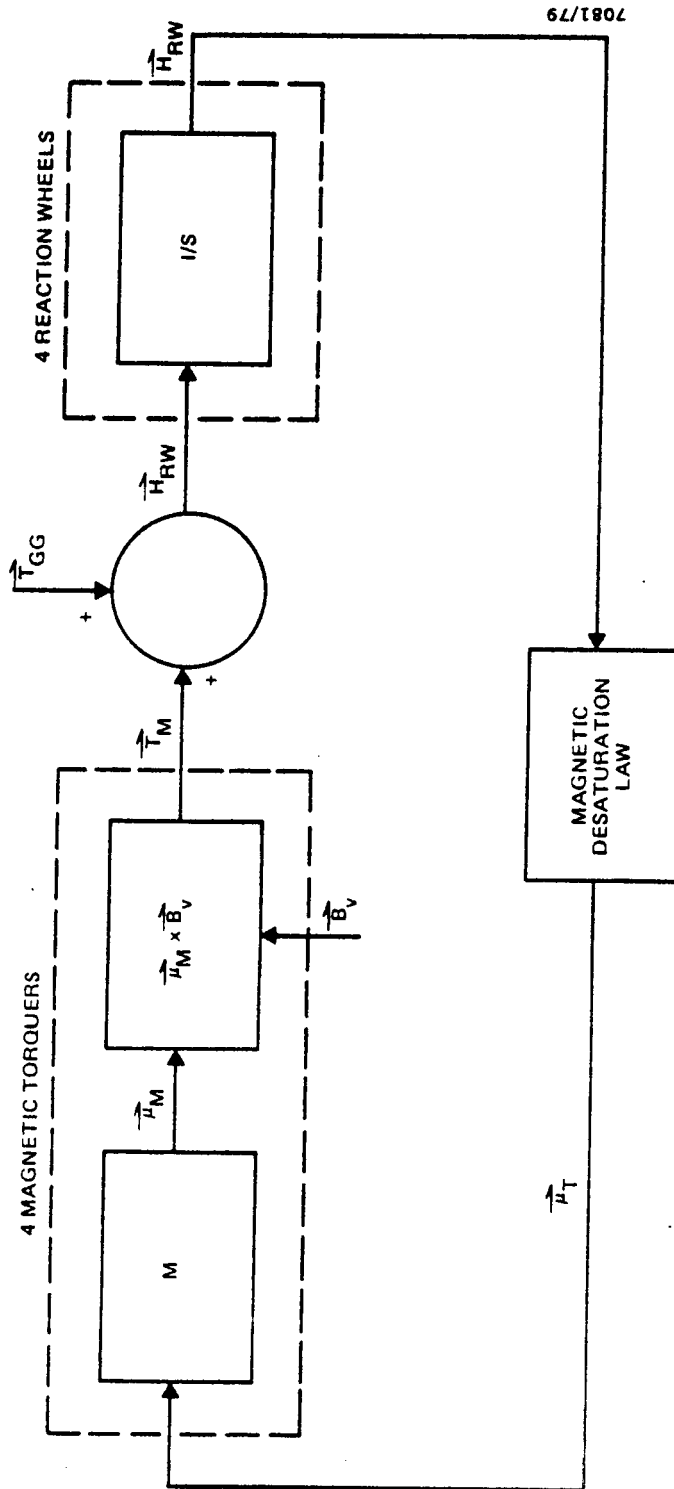
Figure 2-1. Interaction of Desaturation Law With ST Components

This magnetic torque $\vec{T}_M$ is the external torque produced by the momentum management desaturation laws to counteract the environmental disturbance torques, which are dominated by the gravity-gradient torque $\vec{T}_{GG}$, and thus to reduce the buildup of the system momentum and to prevent the reaction wheel speed saturation. It is evident from Equation (2-2) that at any instant no magnetic torque can be produced in the direction of the geomagnetic field. Only because the direction of the geomagnetic field changes in the course of an orbit can dumping of momentum occur in three axes.

With the ST in an inertial attitude, all external torques are absorbed by the reaction wheels. That is,

$$\dot{\vec{H}}_{RW} = \vec{T}_M + \vec{T}_{GG} \qquad (2-3)$$

The dumping of reaction wheel momentum $\vec{H}_{RW}$ is thus achieved by the magnetic torque $\vec{T}_M$ through Equation (2-3). The momentum dumping process results in a new reaction wheel momentum which is fed back to the momentum management desaturation laws for the computation of the next desaturation loop. Equation (2-3) can be generalized to cover the cases of maneuvers by replacing $\vec{H}_{RW}$ by the total system momentum $\vec{H}_T$. That is,

$$\dot{\vec{H}}_T = \dot{\vec{H}}_{RW} + \dot{\vec{H}}_V = \vec{T}_M + \vec{T}_{GG} \qquad (2-4)$$

where $\vec{H}_V$ is the vehicle momentum.

The four reaction wheels are mounted in a configuration as shown in Figure 1-2. The relation between the total reaction wheel system momentum and the individual RW angular velocities, $\vec{\omega}_{RW}$, are given by

$$\vec{H}_{RW} = \begin{bmatrix} a & -a & a & -a \\ -b & -b & b & b \\ -b & -b & -b & -b \end{bmatrix} I_{RW}\vec{\omega}_{RW} = WI_{RW}\vec{\omega}_{RW} \qquad (2\text{-}5)$$

where $a = \sin 20^\circ$, $b = (1/\sqrt{2})\cos 20^\circ$, I_{RW} is the reaction wheel inertia, and the matrix W is called the reaction wheel mounting matrix.

Since the method of Lagrange multipliers is used in the derivation of both the CP law and the ME law, the mathematics used in this method is outlined below. The problem is a minimization problem of the general form

$$J = h(\vec{x}(t_f)) + \int_{t_0}^{t_f} g(\dot{\vec{x}},\vec{x},\vec{u})\, dt \qquad (2\text{-}6)$$

with the constraint

$$f(\dot{\vec{x}},\vec{x},\vec{u},t) = 0 \qquad (2\text{-}7)$$

The necessary conditions for a minimum of J are

$$\frac{\partial g_a}{\partial \vec{x}} - \frac{d}{dt}\left(\frac{\partial g_a}{\partial \dot{\vec{x}}}\right) = 0 \qquad (2\text{-}8)$$

$$\frac{\partial g_a}{\partial \vec{u}} = 0 \qquad (2\text{-}9)$$

$$\frac{\partial g_a}{\partial \vec{x}}\Bigg|_{t = t_f} = 0 \quad \text{(boundary condition)} \qquad (2\text{-}10)$$

where

$$g_a = g(\dot{\vec{x}}, \vec{x}, \vec{u}) + \left(\frac{\partial h}{\partial \vec{x}}\right)^T \dot{\vec{x}} + \vec{P}^T \vec{f}(\dot{\vec{x}}, \vec{x}, \vec{u}, t) \qquad (2\text{-}11)$$

and where $\vec{x}$ = state vector

$\vec{u}$ = independent (control) variable

$\vec{P}$ = costate vector (Lagrange multipliers)

2.2 CROSS PRODUCT CONTROL LAW

The CP law is a closed-loop control law with the actuating signal proportional to the error signal. In other words, it provides the commanded momentum dipole moments, based on the measured reaction wheel momentum, to achieve the momentum desaturation instantaneously.

The original CP law is a simple control law which generates a control dipole along the direction perpendicular to the geomagnetic field with the assumption that the vehicle is in an inertial attitude, i.e., that all external torques are absorbed by the reaction wheels. This CP law is later modified (Reference 2-2) to (1) use the total system momentum $\vec{H}_T$ rather than the RW momentum $\vec{H}_{RW}$ for absorption of the external torques (i.e., use Equation (2-4) rather than Equation (2-3)) so that the law can be used for both maneuvers and observations; (2) minimize the norm of the reaction wheel speed vector to keep the reaction wheel speed during an observation minimal; and (3) add the reaction wheel center speed control loop so that the RW speeds will automatically center after a maneuver and remain centered during an observation. The derivation of the modified CP law, which will be used onboard the ST, is given below.

At any given time in the orbit, the desired magnetic torque, $\vec{T}_D$, is the one that cancels the gravitational gradient torque $\vec{T}_{GG}$ and reduces the total system momentum $\vec{H}_T$. From Equation (2-4), by changing $\vec{T}_M$ to $\vec{T}_D$ and choosing the desired change in $\vec{H}_T$, $\dot{\vec{H}}_T$, to be in the direction of but opposite to $\vec{H}_T$,

$$\vec{T}_D = - \vec{T}_{GG} - K_M \dot{\vec{H}}_T \qquad (2-12)$$

where K_M is the positive constant commonly called the magnetic gain.

However, $\vec{T}_D$ given in Equation (2-12) cannot always be achieved by the magnetic torquers because the magnetic torque $\vec{T}_M$ given by Equation (2-2) has to be perpendicular to the geomagnetic field. One way of determining $\vec{T}_M$ is to let

$$\vec{T}_M = \begin{bmatrix} K_1 & 0 & 0 \\ 0 & K_2 & 0 \\ 0 & 0 & K_3 \end{bmatrix} \vec{T}_D \tag{2-13}$$

and to determine the gain factors K_1, K_2, and K_3 by minimizing the mean square reaction wheel speed, $\vec{\omega}_{RW}^T \vec{\omega}_{RW}$, under the constraint

$$\vec{T}_M \cdot \vec{B} = 0 \tag{2-14}$$

From the minimum norm reaction wheel momentum distribution law (Reference 2-2), $\vec{\omega}_{RW}^T \vec{\omega}_{RW}$ is minimum when expressed in the following form:

$$\vec{\omega}_{RW}^T \vec{\omega}_{RW} = \frac{1}{I_{RW}^2} \vec{H}_{RW}^T \left(WW^T \right)^{-1} \vec{H}_{RW}$$

$$= \frac{1}{4b^2 I_{RW}^2} \vec{H}_{RW}^T \begin{bmatrix} b^2/a^2 & 0 & 0 \\ 0 & 1 & 0 \\ 0 & 0 & 1 \end{bmatrix} \vec{H}_{RW} \tag{2-15}$$

where a and b are defined in Equation (2-5).

Since the resulting RW angular momentum $\vec{H}_{RW}$ during an observation is proportional to the difference between the desired magnetic torque $\vec{T}_D$ and the actual magnetic torque $\vec{T}_M$, it is seen from Equations (2-13) and (2-15) that $\vec{\omega}_{RW}^T \, \vec{\omega}_{RW}$ can be minimized by minimizing the quantity

$$\left[\frac{b}{a} T_{D_1} (K_1 - 1)\right]^2 + \left[T_{D_2} (K_2 - 1)\right]^2 + \left[T_{D_3} (K_3 - 1)\right]^2 \qquad (2\text{-}16)$$

subject to the constraint of Equation (2-14), i.e.,

$$K_1 T_{D_1} B_1 + K_2 T_{D_2} B_2 + K_3 T_{D_3} B_3 = 0 \qquad (2\text{-}17)$$

Applying the method of Lagrange multipliers gives

$$2 \left(\frac{b}{a} T_{D_1}\right)^2 (K_1 - 1) + \lambda \, T_{D_1} B_1 = 0$$

$$2 T_{D_2}^2 (K_2 - 1) + \lambda \, T_{D_2} B_2 = 0 \qquad (2\text{-}18)$$

$$2 T_{D_3}^2 (K_3 - 1) + \lambda \, T_{D_3} B_3 = 0$$

$$T_{D_1} B_1 K_1 + T_{D_2} B_2 K_2 + T_{D_3} B_3 K_3 = 0$$

where λ is the Lagrange multiplier.

Solving for K_1, K_2, K_3, and λ from Equation (2-18) yields

$$K_1 = 1 - \frac{\left(\frac{a}{b}\right)^2 B_1 \, \vec{T}_D \cdot \vec{B}}{T_{D_1} \, \vec{B}' \cdot \vec{B}}$$

$$K_2 = 1 - \frac{B_2 \, \vec{T}_D \cdot \vec{B}}{T_{D_2} \, \vec{B}' \cdot \vec{B}}$$

$$K_3 = 1 - \frac{B_3 \, \vec{T}_D \cdot \vec{B}}{T_{D_3} \, \vec{B}' \cdot \vec{B}}$$

$$\lambda = \frac{2\vec{T}_D \cdot \vec{B}}{\vec{B}' \cdot \vec{B}}$$

(2-19)

where

$$\vec{B}' \equiv \left[\left(\frac{a}{b}\right)^2 B_1, \; B_2, \; B_3 \right]^T$$

Substituting Equation (2-19) into Equation (2-13) gives

$$\vec{T}_M = \vec{T}_D - \frac{\vec{T}_D \cdot \vec{B}}{\vec{B}' \cdot \vec{B}} \, \vec{B}'$$

$$= \frac{\left(\vec{B}' \times \vec{T}_D\right) \times \vec{B}}{\vec{B}' \cdot \vec{B}}$$

(2-20)

Hence, by comparing Equation (2-20) with Equation (2-2),

$$\vec{\mu}_M = \frac{\vec{B}' \times \vec{T}_D}{\vec{B}' \cdot \vec{B}} \qquad (2-21)$$

Substituting Equation (2-15) into Equation (2-1) results in

$$M\vec{\mu}_T = \frac{\vec{B}' \times \vec{T}_D}{\vec{B}' \cdot \vec{B}} \qquad (2-22)$$

According to the pseudo-inverse law, the power loss in the magnetic coil will be minimal if the magnetic moment is distributed among the four electromagnets by the following:

$$\vec{\mu}_T = M^T \left(MM^T\right)^{-1} \frac{\vec{B}' \times \vec{T}_D}{\vec{B}' \cdot \vec{B}} \qquad (2-23)$$

Thus, the basic CP law for both observations and maneuvers is obtained by substituting Equation (2-12) into Equation (2-23).

$$\vec{\mu}_T = -M^T \left(MM^T\right)^{-1} \frac{\vec{B}' \times \left[\vec{T}_{GG} + K_M \left(W I_{RW} \vec{\omega}_{RW} + I_V \vec{\omega}_V\right)\right]}{\vec{B}' \cdot \vec{B}} \qquad (2-24)$$

where $\vec{T}_{GG}$ = calculated vehicle gravitational gradient torque

$\vec{\omega}_{RW}$ = sensed reaction wheel speeds

$\vec{\omega}_V$ = sensed vehicle rate

$\vec{B}$ = sensed Earth magnetic field

I_V = vehicle inertia matrix

I_{RW} = reaction wheel inertia matrix

Computer studies show that $K_M = 2 \Omega_o$ (Ω_o = orbital rate) minimizes the reaction wheel speed swings during an observation.

The CP law given in Equation (2-24) is further modified by incorporating the reaction wheel center speed control loops to keep the reaction wheel center speeds at zero. This results in (Reference 2-2) adding two additional terms in $\vec{T}_D$. That is,

$$\vec{T}_D = - \vec{T}_{GG} - K_M \left(\vec{H}_T + K_P \vec{H}_{CSD} + K_\Sigma \vec{\Sigma} \right) \tag{2-25}$$

where $\vec{H}_{CSD}$ is the RW center speed momentum with dead zone, $\vec{\Sigma}$ is the sum of the RW center speed momenta with limits ($\vec{H}_{CSL}$) for all passes through the CP law, and K_p and K_Σ are constants. The momentum vectors $\vec{H}_{CSD}$ and $\vec{\Sigma}$ are defined in the following:

$$
\begin{aligned}
\left(H_{CSD} \right)_1 &= 0 && \text{if } \left| \left(H_{CS} \right)_1 \right| \leq H_{NL1} \\
&= \left(H_{CS} \right)_1 - H_{NL1} && \text{if } \left(H_{CS} \right)_1 > H_{NL1} \\
&= \left(H_{CS} \right)_1 + H_{NL1} && \text{if } \left(H_{CS} \right)_1 < - H_{NL1}
\end{aligned}
$$

$$
\begin{aligned}
\left(H_{CSD} \right)_i &= 0 && \text{if } \left| \left(H_{CS} \right)_i \right| \leq H_{NL2} \\
&= \left(H_{CS} \right)_i - H_{NL2} && \text{if } \left(H_{CS} \right)_i > H_{NL2} \\
&= \left(H_{CS} \right)_i + H_{NL2} && \text{if } \left(H_{CS} \right)_i < - H_{NL2} \quad (i = 2, 3)
\end{aligned}
$$

$$\tag{2-26}$$

$$
\begin{aligned}
\left(H_{CSL} \right)_1 &= \left(H_{CS} \right)_1 && \text{if } \left| \left(H_{CS} \right)_1 \right| \leq H_{NL1} \\
&= H_{NL1} && \text{if } \left(H_{CS} \right)_1 > H_{NL1} \\
&= - H_{NL1} && \text{if } \left(H_{CS} \right)_1 < - H_{NL1}
\end{aligned}
$$

2-11

$$\left(H_{CSL}\right)_i = \left(H_{CS}\right)_i \quad \text{if } \left|\left(H_{CS}\right)_i\right| \leq H_{NL2}$$

$$= H_{NL2} \quad \text{if } \left(H_{CS}\right)_i > H_{NL2}$$

$$= -H_{NL2} \quad \text{if } \left(H_{CS}\right)_i < -H_{NL2} \qquad (i = 2, 3)$$

$$\vec{\Sigma} = \Sigma \, \vec{H}_{CSL} \quad \text{(sum over all passes through the CP law)}$$

where
$$\vec{H}_{CS} = \text{total system momentum due to RW center speeds}$$

$$= W \, I_{RW} \, \vec{\omega}_{CS}$$

$$\vec{\omega}_{CS} = 1/2 \left(\vec{\omega}_{RW_{MAX}} + \vec{\omega}_{RW_{MIN}}\right)$$

$$\vec{\omega}_{RW_{MAX}} = \text{maximum RW speed over last half orbit}$$

$$\vec{\omega}_{RW_{MIN}} = \text{minimum RW speed over last half orbit}$$

$$H_{NL1} = \text{RW center speed control loop first axis nonlinearities breakpoint}$$

$$H_{NL2} = \text{RW center speed control loop second and third axes nonlinearities breakpoint}$$

The relations between $\vec{H}_{CSD}$, $\vec{H}_{CSL}$, and $\vec{H}_{CS}$ given in Equation (2-26) are shown in Figure (2-2). The nominal values for H_{NL1}, H_{NL2}, K_P and K_Σ are determined to be:

$$H_{NL1} = 10.2$$
$$H_{NL2} = 19.8$$
$$K_P = 2.828 \qquad\qquad (2-27)$$
$$K_\Sigma = 0.06659$$

with all quantities expressed in MKS units.

2.2.1 Description of Onboard Implementation

The ST onboard software requirements are described in References 2-3 and 2-4. The onboard implementation of the CP desaturation law is summarized in Figure 2-3. A RW center speed computation module and a gravity-gradient model
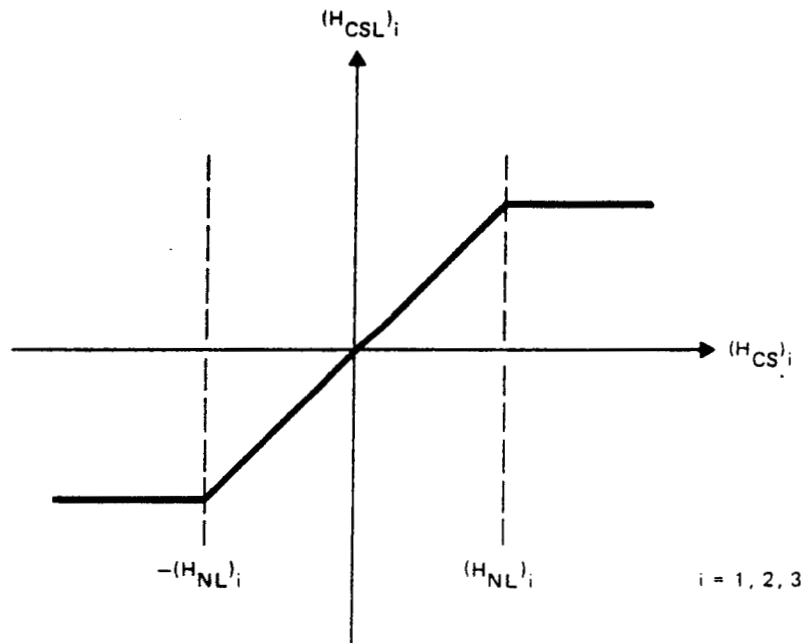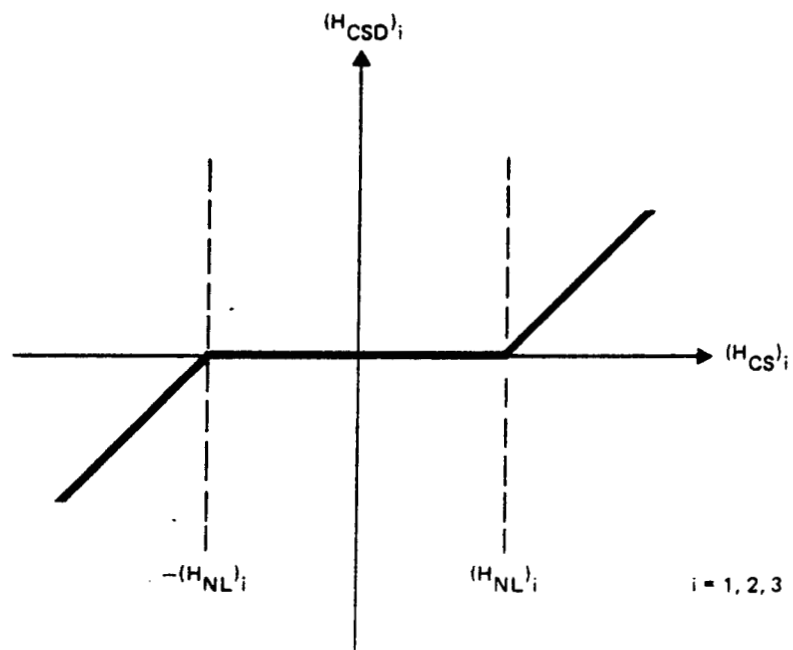
$(H_{NL})_1 = H_{NL1}$

$(H_{NL})_2 = (H_{NL})_3 = H_{NL2}$

7081/79

Figure 2-2. Definition of RW Center Speed Momentum Vectors

2-13
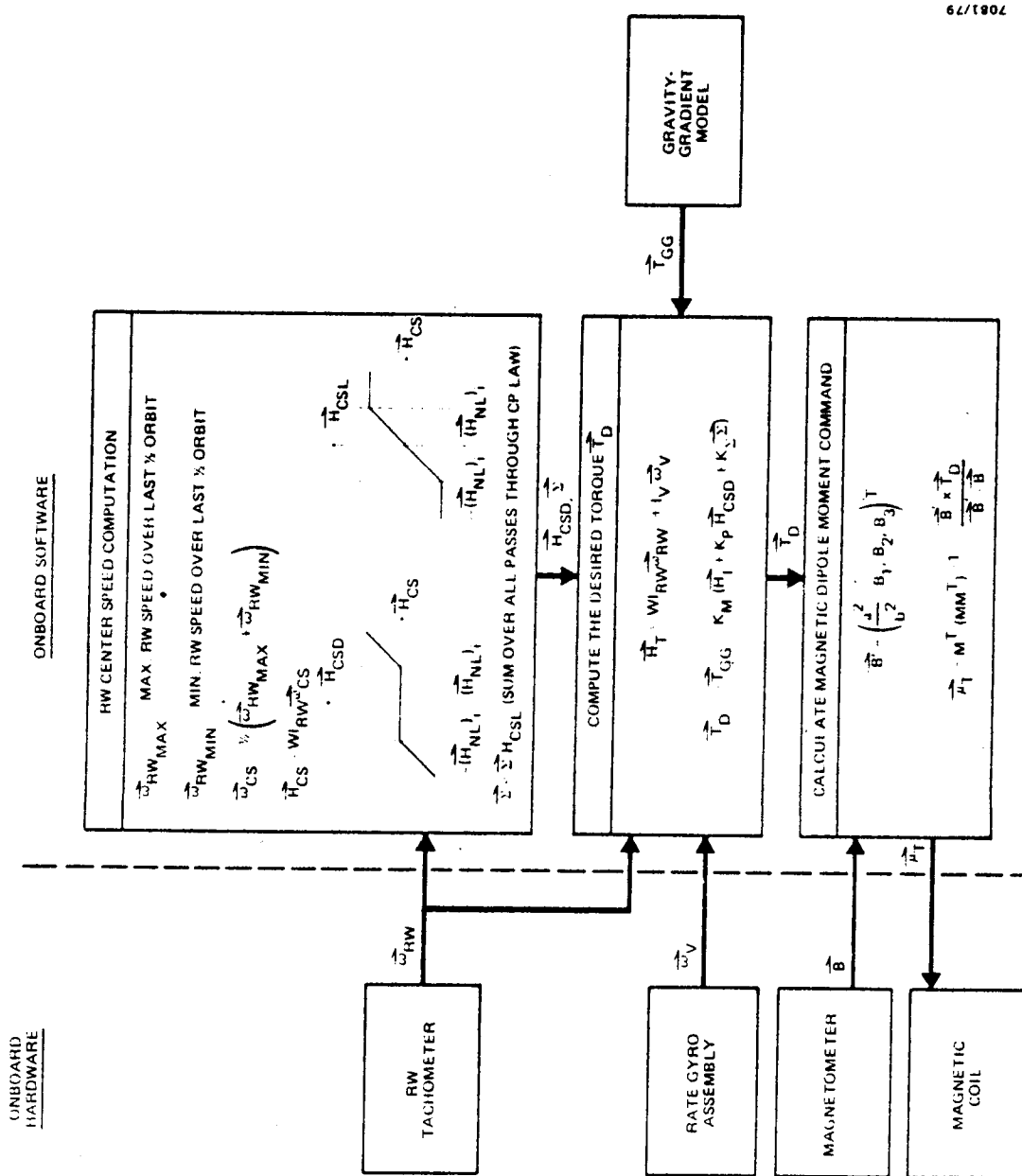
Figure 2-3. Baseline Diagram of Onboard CP Law Implementation

2-14

must be implemented onboard to compute the desired torque $\vec{T}_D$. The RW center speed computation module computes the vectors $\vec{H}_{CSD}$ and $\vec{\Sigma}$ necessary for the RW center speed control based on the RW speed measurements $\vec{\omega}_{RW}$ sensed by the RW tachometer over the last half-orbit period. With $\vec{H}_{CSD}$ and $\vec{\Sigma}$ computed, the desired torque $\vec{T}_D$ is then calculated using the gravity-gradient torque $\vec{T}_{GG}$ obtained from the gravity-gradient model and the RW speed and vehicle speed sensed by the RW tachometer and the rate gyro assembly (RGA), respectively. After $\vec{T}_D$ is computed, the magnetic dipole moment command $\vec{\mu}_T$ is then calculated, using the geomagnetic field sensed by the magnetometer, and sent to the magnetic coils to generate the magnetic torque necessary for the momentum desaturation.

2.2.2 Required Support by the Ground System

As shown in Figure 2-3, the implementation of the CP law requires essentially no support from the ground system. However, because of the finite possibility that the RWA speed may exceed the 10-hertz limit using the CP law, a simulator on the ground may be necessary for target screening and control law selection. This will not only increase the amount of ground software support, but also cause some operational impact. Therefore, it is recommended that further studies be performed to define the cases where the CP law is not applicable so that the necessity of the simulator can be removed. More discussion regarding this subject is given in Section 4.

2.3 MINIMUM ENERGY CONTROL LAW

2.3.1 Derivation of Minimum Energy Control Law

The ME control law is designed to minimize the energy required by the magnetic torquers to dump a given amount of angular momentum during a specified time interval called the desaturation period. The equations derived in this subsection are limited to the cases of inertial attitudes. For the cases of slew maneuvers, proper coodinate transformations from momentary spacecraft coordinates to inertial coordinates are required (Reference 2-5).

The energy lost in the magnetic coils within a desaturation period of t_o to t_f is given by

$$E = \frac{k}{2} \int_{t_o}^{t_f} \vec{\mu}_T^T \, \vec{\mu}_T \, dt \tag{2-28}$$

where k is a constant.

From Equations (2-1) to (2-3), the magnetic dipole moment $\vec{\mu}_T$ is subject to the following differential equation constraint:

$$\widetilde{B} \, M \, \vec{\mu}_T - \vec{T}_{GG} + \dot{\vec{H}}_{RW} = \vec{O} \tag{2-29}$$

where

$$\widetilde{B} = \begin{bmatrix} 0 & -B_3 & B_2 \\ B_3 & 0 & -B_1 \\ -B_2 & B_1 & 0 \end{bmatrix} \tag{2-30}$$

2-16

Thus, the ME law is to determine the magnetic dipole moment vector $\vec{\mu}_T$ by minimizing the quantity E given by Equation (2-28) subject to the constraint of Equation (2-29). Applying the method of Lagrange multipliers, Equation (2-11) gives

$$g_a = k\left[\frac{1}{2}\vec{\mu}_T^T\ \vec{\mu}_T + \vec{P}^T\ (\widetilde{B}\ M\vec{\mu}_T - \vec{T}_{GG} + \dot{\vec{H}}_{RW})\right] \qquad (2\text{-}31)$$

Then, from Equations (2-8) and (2-9), the following necessary conditions are derived:

$$\frac{d}{dt}\ (\vec{P}) = 0 \qquad (2\text{-}32)$$

$$\vec{\mu}_T + M^T\ \widetilde{B}^T\ \vec{P} = 0 \qquad (2\text{-}33)$$

Equation (2-32) implies that $\vec{P}$, the vector of Lagrange multipliers or the costate vector, is constant. Solving for $\vec{\mu}_T$ from Equation (2-33) gives

$$\begin{aligned}
\vec{\mu}_T &= -M^T\ \widetilde{B}^T \cdot \vec{P} \\
&= M^T\ \widetilde{B}\ \vec{P} \\
&= M^T\ \vec{B} \times \vec{P}
\end{aligned} \qquad (2\text{-}34)$$

Substituting Equation (2-34) into Equation (2-29) and integrating over the desaturation period yields

$$\vec{H}_{RW}(t_f) - \vec{H}_{RW}(t_o) = \int_{t_o}^{t_f} \widetilde{B} \, M \, M^T \, \widetilde{B}^T \, dt \, \vec{P}$$

$$+ \int_{t_o}^{t_f} \vec{T}_{GG} \, dt$$

(2-35)

Solving for $\vec{P}$ from Equation (2-35) gives

$$\vec{P} = \left[\int_{t_o}^{t_f} \widetilde{B} \, M \, M^T \, \widetilde{B}^T \, dt \right]^{-1} \vec{H}_D$$

(2-36)

where

$$\vec{H}_D = \vec{H}_{RW}(t_f) - H_{RW}(t_o) - \int_{t_o}^{t_f} \vec{T}_{GG} \, dt$$

(2-37)

The ME desaturation law is presented by Equations (2-34), (2,36), and (2-37). The momentum $\vec{H}_D$ defined in Equation (2-37) is the total momentum to be dumped during the desaturation interval t_o to t_f.

2.3.2 Description of Onboard Implementation

2.3.2.1 Implementation of the ME Law

The ME law was originally developed by Dr. John Glaese et al. (Reference 2-6). The conventional implementation of the ME law is to use a half-orbit period as the desaturation interval and to update the costate vector $\vec{P}$ at the end of each desaturation period. The RW system momentum at the end of each desaturation interval, $\vec{H}_{RW}(t_f)$, is constant and is selected to center the positive and negative RW speed excursions. This implementation is schematically shown in Figure 2-4(a). The desaturation period is set at half an orbit period to include the major variations in the geomagnetic field and to be compatible with the period of gravity-gradient disturbances. The result is that only the nonperiodic portion of the accumulated gravity-gradient momentum is dumped, and no attempt is made to counteract the periodic portion.

Since the ME desaturation law is open-loop in nature (that is, the RW system momentum $\vec{H}_{RW}$ couples into the desaturation law only at the beginning of a desaturation period), a desaturation interval of as long as half an orbit period can allow $\vec{H}_{RW}$ to drift to large values in the presence of offnominal conditions such as coil or RW failures. Thus, the conventional ME law only performs satisfactorily if either no failure conditions are present or if only detected failure conditions are present. To resolve this problem, it is necessary to modify the implementation of the conventional ME law.

The purpose of the modification is to reduce the drawback of the open-loop process by shortening the desaturation period and increasing the updating frequency of the costate vector computation, while at the same time keeping the advantages of using the half-orbit period as the desaturation interval by replacing the $\vec{H}_{RW}(t_f)$ in Equation (2-37) with a nominal RW system momentum $\vec{H}_{NOM}(t_f)$. This nominal momentum profile $\vec{H}_{NOM}(t)$ is the RW system momentum time history obtained from the conventional ME law with a half-orbit desaturation period and updating interval. $\vec{H}_{NOM}(t)$ can be approximated by a first-order

Fourier expansion. The Fourier coefficients will be computed on the ground and uplinked to the ST. The computation of $\vec{H}_{NOM}$ (t) is discussed in detail in Section 3.

Based on a parametric study performed by LMSC (Reference 2-1), the values of the desaturation period and the costate vector updating interval for the modified ME control law have been recommended to be 600 seconds and 200 seconds, respectively.

The equations used in the modified ME control law are summarized below:

$$\vec{\mu}_T = M^T \, \tilde{B} \, \vec{P}$$

$$\vec{P} = \left[\int_{t_o}^{t_f} \tilde{B} \, M \, M^T \, \tilde{B}^T \, dt \right]^{-1} \vec{H}_D$$

$$\vec{H}_D = \vec{H}_{NOM} \, (t_f) - \vec{H}_{RW} \, (t_o) - \int_{t_o}^{t_f} \vec{T}_{GG} \, dt$$

(2-38)

$$t_f = t_o + 600 \text{ seconds}$$

where t_o is incremented in steps of 200 seconds and $\vec{H}_{NOM}$ (t) is the nominal RW system momentum obtained with a half-orbit desaturation period. The implementation of this modified ME control law is shown in Figure 2-4(b). It is much closer to a closed-loop process than the conventional ME law. However, the resulting RW system momentum is identical with what would have been obtained under the nominal situation if the conventional implementation of the ME law were used.

The implementation of the ME law discussed above is limited to the case of inertial attitudes. For the case of slew maneuvers, the implementation is
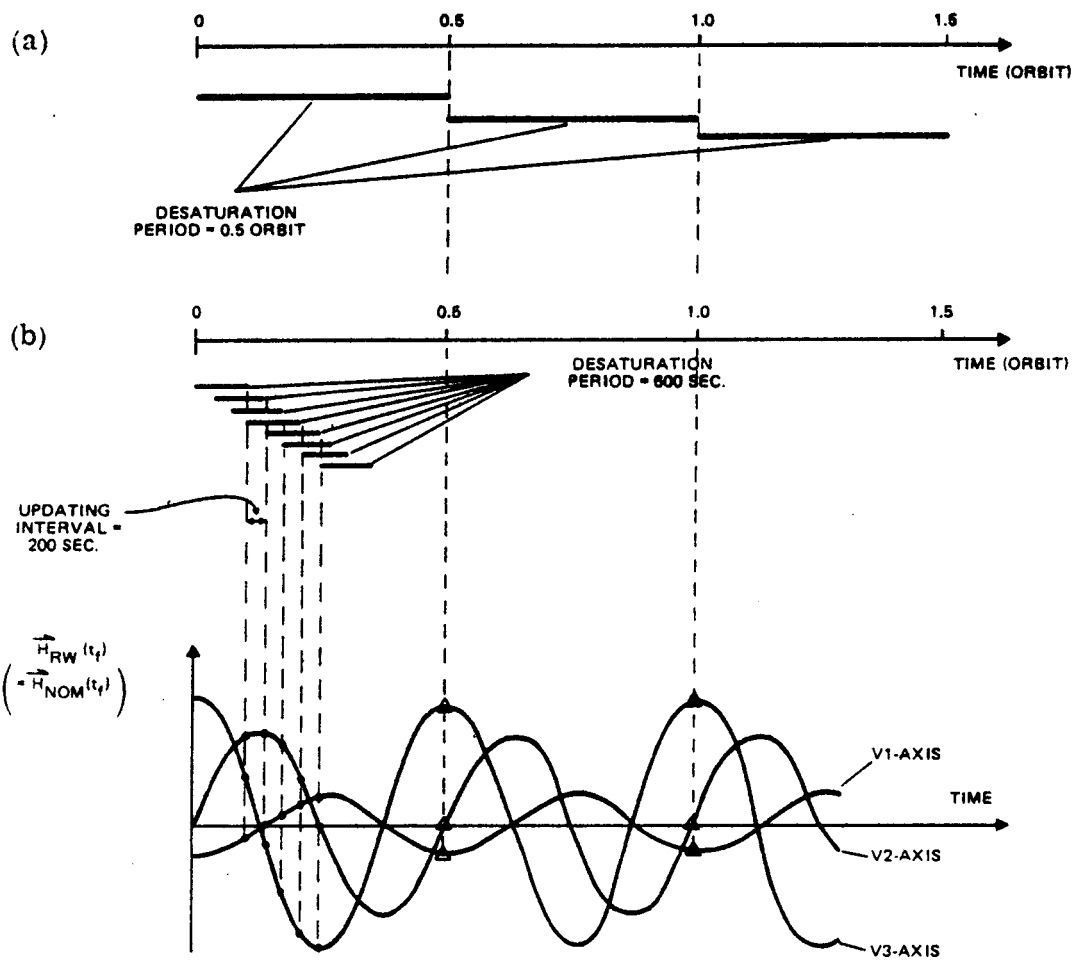
Figure 2-4.   Implementation of ME Control Law
            (a) Conventional Implementation
            (b) Modified Implementation

somewhat different (Reference 2-5). A short time before the start of a slew maneuver (called the lead time), the normal mode of the ME process is interrupted and a separate maneuver desaturation interval is initiated. This maneuver desaturation interval spans the entire maneuver and ends a short time after the end of the maneuver (called the lag time). At the termination of the maneuver desaturation interval, the ME law continues with its normal mode of 600-second intervals and 200-second updates. This mechanization is schematically shown in Figure 2-5(a). When two slew maneuvers are closely spaced, the lag time at the end of one maneuver may overlap the lead time of the next maneuver. In this case, the first maneuver desaturation interval is set up in the same way as for a single maneuver, whereas the second maneuver desaturation interval starts halfway between the two maneuvers. This is schematically shown in Figure 2-5(b). When the end of one desaturation interval occurs within a maneuver, that maneuver is ignored in computing the ME law and it is assumed that the ST attitude is still that of the inertial attitude prior to the maneuver. The advantage of this technique of implementing the ME law during maneuvers is that the end of a desaturation interval never falls within a slew maneuver and therefore there is no need of computing the nominal momentum for a time-varying attitude. This significantly simplifies the nominal momentum computations because the nominal momentum can be represented by a sinusoidal function when the ST is in an inertial attitude.

The required lengths of the lead and lag times have been studied by LMSC. It was found that the minimum required lengths for worst case maneuvers do not vary much with slew angle for values above 30 degrees. They are about 500 seconds for the orbit tracks that are favorable for momentum dumping and about 900 seconds for the unfavorable orbit tracks. For slew angles below 30 degrees, the lead and lag times can be linearly decreased with slew angle. For most of the maneuvers to be executed by the ST, the minimum required lead and lag times will be shorter than that stated above. However, it was
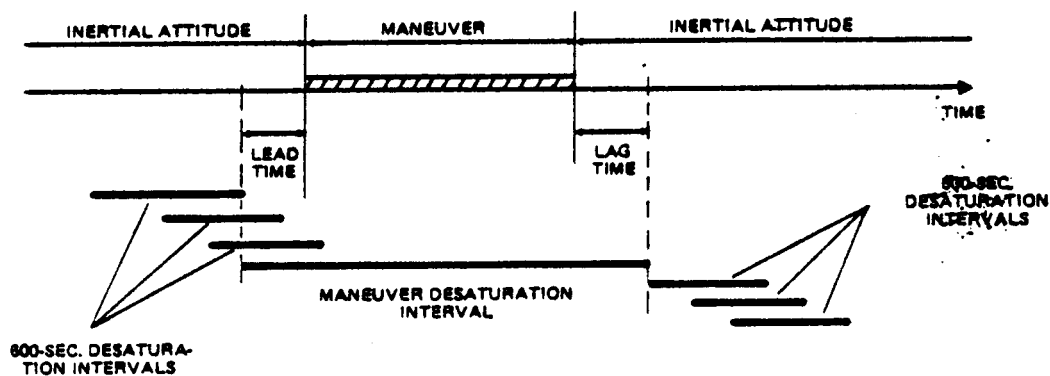
(a)
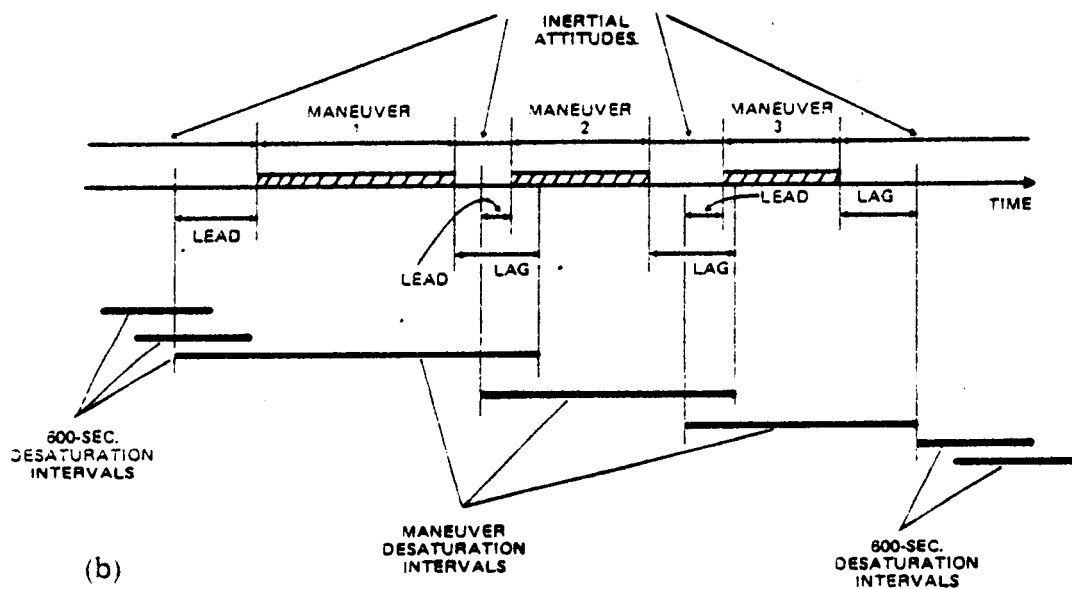
(b)

Figure 2-5. Desaturation Intervals

  (a) For a Single Maneuver

  (b) For a Series of Closely
      Spaced Maneuvers

found that the peak RWA speeds are not sensitive to the lengths of the lead and lag times and therefore no real benefit would result from using the minimum required lengths of the lead and lag times for each maneuver. The procedure for selecting the lead and lag times will be implemented at the STOCC and the lead and lag times will be made part of the maneuver command list.

2.3.2.2 System Baseline

Figure 2-6 is a baseline diagram of the onboard implementation of the ME desaturation law. In the figure, the coordinate transformation matrix $\Gamma_{t,t'}$, which is computed onboard by a command generator, is included in the equations to cover the cases of maneuvers. In the case of inertial attitude, $\Gamma_{t,t'}$ equals identity. The geomagnetic field model, the gravity-gradient model, and the Fourier expansion of the nominal RW system momentum must be stored onboard for the purpose of computing the costate vector $\vec{P}$. The RW momentum at the start of each desaturation period, $\vec{H}_{RW}(t_o)$, is obtained from the $\vec{\omega}_{RW}$ measurement sensed by the RW tachometer. During an observation, $\vec{P}$ is computed with desaturation periods, $t_f - t_o$, of 600 seconds and updated every 200 seconds. For the case of maneuvers, $\vec{P}$ is computed for a desaturation interval from maneuver start time minus lead time to maneuver end time plus lag time with no updates. The lead and lag times of each maneuver are predetermined by the STOCC and sent to the ST as part of the maneuver commands.

After $\vec{P}$ is computed, the magnetic dipole moment command $\vec{\mu}_T$ is then calculated using the geomagnetic field model and sent to the magnetic coils to generate the desired magnetic torque. The updating frequency of $\vec{\mu}_T$ is every 50 seconds. For the case of maneuvers, the inertially fixed $\vec{P}$ must be transformed to the instantaneous body coordinates before $\vec{\mu}_T$ is computed. This coordinate transformation is performed by using the vehicle angular velocity measured by the rate gyro assembly.
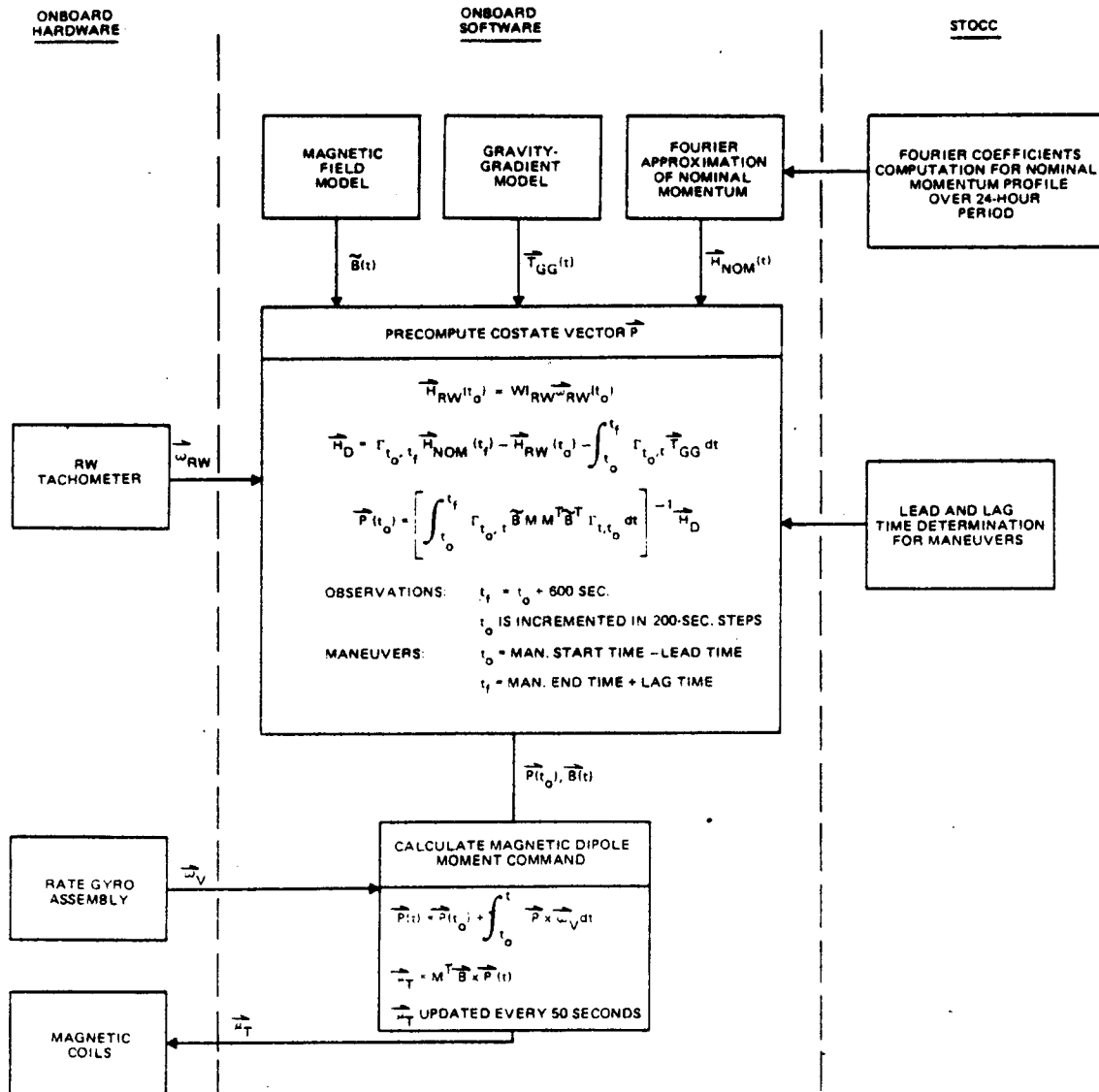
Figure 2-6. Baseline Diagram of Onboard ME Law Implementation

2.3.3 Required Support by the Ground System

The required support by the ground system (STOCC) for the momentum management using the ME control law can be categorized into three items: (1) the computation of the Fourier coefficients for the nominal momentum profile $\vec{H}_{NOM}$ for all the inertial attitudes covering the 24-hour period; (2) the determination of the lengths of the lead and lag times for each of the slew maneuvers; and (3) the screening of targets based on the requirement that the reaction wheel speeds have to remain below approximately 10 hertz while the ST is in the fine pointing mode.

The Fourier coefficients for the nominal momentum profile are needed because of the modification to the conventional ME law as discussed in Section 2.3.2.1. The analytical considerations necessary for this implementation are given in detail in Section 3. The determination of the lead and lag times for maneuvers is required by the way the desaturation period is defined for the maneuvers (see Section 2.3.2.1 and Figure 2-5). The screening of targets is necessary because, based on the simulation studies performed by LMSC (Reference 2-5), finite chances (~5 percent if all RWA are operational and ~15 percent when one RWA failed) exist in having the RWA speed exceed the 10-hertz limit during the lead and lag time of a maneuver.

Both the determination of the lead and lag times and the screening of targets can be achieved by implementing a simulation for the ME control law. This problem is further discussed in Section 4.

REFERENCES

2-1. Lockheed Missiles and Space Company, LMSC-HREC TM D 496086, Reaction Wheel Speed Minimization through Mangetic Desaturation, A. Wernli, November 1976

2-2. --, SE-03, Section H, "Space Telescope Project Support Systems Module, Appendix 5, Cross-product Momentum Management," April 1979

2-3. --, LMSC 4171856A, Space Telescope Flight Software Requirements, R. H. Jones, W. F. Wright, W. H. Whittier, October 1979

2-4. --, LMSC 4172682, ST PCS Flight Software Algorithms, R. H. Jones, W. F. Wright, W. H. Whittier, October 1979

2-5. --, SE-03, Section H, "Space Telescope Project Support Systems Module, Appendix 6, Minimum-Energy Momentum Management," April 1979

2-6. J. R. Glaese, et al., "Low-Cost Space Telescope Pointing Control System," J. Spacecraft, vol. 13, no. 7, July 1976

SECTION 3 - ANALYTICAL CONSIDERATION FOR GROUND SUPPORT
OF THE ME CONTROL LAW

The computational support to be performed in the STOCC for the ME control law is the determination of the nominal angular momentum profile, $\vec{H}_{NOM}(t)$. $\vec{H}_{NOM}(t)$ is the momentum time history of a nominally operating spacecraft driven by the ME control law with a half-orbit desaturation period. The values of $\vec{H}_{NOM}(t)$ will be used onboard as the target momentum toward which the reaction wheel system momentum will be continuously driven under the modified ME control law, which has a 600-second desaturation period and a 200-second updating interval. The significance of the half-orbit desaturation period used in determining $\vec{H}_{NOM}(t)$ is to provide a sufficiently long period so that a sizable variation in the direction of the geomagnetic field will occur to make the desired momentum unloading possible and to take advantage of the half-orbit period of the cyclic gravity-gradient torque components. The much shorter desaturation period and updating interval to be used onboard will shorten the open-loop desaturation process to prevent the reaction wheel momentum from drifting to very large values in the presence of off-nominal conditions.

The manner in which momentum unloading is performed during slew maneuvers does not require a nominal momentum profile for the duration of the maneuver. The nominal momentum profile is only required for inertial attitudes.

3.1 OVERVIEW OF COMPUTATION SEQUENCE

Since the nominal momentum profile is periodic with one-half orbit, it can be approximated by a sinusoidal function of the following form:

$$\vec{H}_{NOM}(t) = \vec{a} \cos \frac{2\pi}{T} t + \vec{b} \sin \frac{2\pi}{T} t$$

where T is the half-orbit period and the components of a and b are the Fourier coefficients to be computed at the STOCC and uplinked to the ST. One set of coefficients is required for each inertial attitude.

The computation sequence for the Fourier coefficients at a given inertial attitude is illustrated in Figure 3-1. In the figure, T_o is the time at the end of the last slew maneuver, h and N are the integration step size and the number of integration steps, respectively, to be used in computing the Fourier coefficients. All other parameters are as defined in Section 2. The computational sequence can be generally divided into three major steps: (1) the computation of the costate vector $\vec{P}$ corresponding to a half-orbit desaturation period; (2) the computation of the nominal momentum time history $\vec{H}_{NOM}$ (t); and (3) the transformation of $\vec{H}_{NOM}$ (t) to the Fourier coefficients $\vec{a}$ and $\vec{b}$.

In each of the three steps, a numerical integration technique is required. The most commonly used numerical integration technique is the fourth-order Runge-Kutta method, which will be discussed in Section 3.2. The integration steps referred to in Figure 3-1 are based on this method. The accuracies of the results depend on the step sizes used. On the basis of simulations using the fourth-order Runge-Kutta method, LMSC has recommended (Reference 3-1) a step size of 600 seconds or less to achieve the 2-percent accuracy requirement on $\vec{H}_{NOM}$. This suggests a value of $N = 5$ for the number of integration steps defined in Figure 3-1.

Besides the integration technique, two areas have to be addressed to carry out the computations outlined in Figure 3-1: the computation of the gravitational gradient torque $\vec{T}_{GG}$ (t) and the computation of the geomagnetic field $\vec{B}$ (t), both represented in the ST body-fixed coordinate system. These are given in Sections 3.3 and 3.4, respectively.

START

COMPUTE GEOMAGNETIC FIELD $\vec{B}(t_n)$
AND GRAVITY-GRADIENT TORQUE $\vec{T}_{GG}(t_n)$

AT

$$t_n = T_o + n\frac{h}{4}, \; n = 0, 1, \ldots, 4N$$

COMPUTE COSTATE VECTOR $\vec{P}$

$$\vec{P} = \left[\int_{T_o}^{T_o + T} \widetilde{B} MM^T \widetilde{B} \, dt \right]^{-1} \left[-\int_{T_o}^{T_o + T} \vec{T}_{GG} \, dt \right]$$

WITH INTEGRATION STEP SIZE $= \frac{h}{2}$

COMPUTE THE MAGNETIC TORQUE, $\vec{T}_M(t_n)$,
RESULTING FROM THE CONTROL ELECTROMAGNETS

$$\vec{T}_M(t_n) = \vec{B}(t_n) \times \left[MM^T (\vec{B}(t_n) \times \vec{P}) \right]$$

AT $t_n = T_o + n\frac{h}{4}, \; n = 0, 1, \ldots, 4N$

COMPUTE THE NOMINAL MOMENTUM PROFILE
$\vec{H}_{NOM}(t_i)$

$$\vec{H}_{NOM}(t_i) = \int_{T_o}^{t_i} \vec{T}_M(t) - \vec{T}_{GG}(t) \, dt$$

AT $t_i = T_o + i\frac{h}{2}, \; i = 0, 1, \ldots, 2N$

INITIAL CONDITION: $\vec{H}_{NOM}(T_o) = \vec{0}$

COMPUTE THE FOURIER COEFFICIENTS $\vec{a}, \vec{b}$

$$\vec{a} = \frac{2}{T} \int_{T_o}^{T_o + T} \vec{H}_{NOM}(t) \cos \left(\frac{2\pi}{T} t \right) dt$$

$$\vec{b} = \frac{2}{T} \int_{T_o}^{T_o + T} \vec{H}_{NOM}(t) \sin \left(\frac{2\pi}{T} t \right) dt$$

INTEGRATION STEP SIZE $= h = T/N$

END

Figure 3-1.   Computation Flow for the Fourier Coefficients of the
Nominal Momentum Profile

3.2 NUMERICAL INTEGRATION TECHNIQUE--FOURTH-ORDER RUNGE-KUTTA METHOD

To integrate a differential equation of the form

$$\frac{dy}{dt} = f(t, y) \tag{3-1}$$

and to obtain an exact close-formed solution for y is usually difficult and most of the time impossible. Techniques to provide numerical approximations are therefore important.

Among the many techniques available in evaluating numerical integrations (e.g., Reference 3-2), the fourth-order Runge-Kutta method is most often used because of its accuracy and simplicity. Therefore, this method is recommended for use by the STOCC to generate the nominal momentum profile. The equations to be used in this method to compute function y are given below without derivations:

$$y_{n+1} = y_n + \frac{h}{6}(k_1 + 2k_2 + 2k_3 + k_4)$$

$$k_1 = f(t_n, y_n)$$

$$k_2 = f(t_n + \frac{h}{2}, y_n + \frac{1}{2}hk_1)$$

$$k_3 = f(t_n + \frac{h}{2}, y_n + \frac{1}{2}hk_2) \tag{3-2}$$

$$k_4 = f(t_n + h, y_n + hk_3)$$

where $t_n = t_0 + nh$, $y_n = y(t_n)$, and h is the step size of the integration.

In the case that f is independent of y, Equation (3-1) becomes

$$y(t) = \int_{t_0}^{t} f(\tau) \, d\tau \qquad (3\text{-}3)$$

and Equation (3-2) reduces to Simpson's rule of numerical integration:

$$y_{n+1} = y_n + \frac{h}{6}\left[f_n + 4 f_{n+h/2} + f_{n+h}\right] \qquad (3\text{-}4)$$

This simplification is appropriate for each of the numerical integrations required in Figure 3-1.

With Equation (3-4), y(t) can be evaluated at any time t by a proper choice of the integration step h. Notice in Equation (3-4) that for a given value of h, the function f is to be computed at both ends of the interval as well as the midpoint between the two ends. Therefore, the actual step size required in computing f is h/2. As shown in Figure 3-1, to obtain the Fourier coefficients $\vec{a}$ and $\vec{b}$ at an integration step size h, the nominal momentum time history $\vec{H}_{NOM}$ (t) must be evaluated at h/2 steps and this requires the computation of $\vec{T}_M$, $\vec{T}_{GG}$, and $\vec{B}$ at h/4 steps.

3.3 COMPUTATION OF GRAVITY-GRADIENT TORQUES

The gravity-gradient torque for computing the nominal momentum profile (Reference 3-1) is given by

$$\vec{T}_{GG} = 3\Omega_0^2 \left[\hat{R}_V \times (\hat{I}\hat{R}_V)\right] \qquad (3\text{-}5)$$

where Ω_0 = spacecraft angular rate

$\qquad$ = π/T, where T = half-orbit period

$\qquad$ I = ST inertia matrix

$\hat{R}_V$ = unit ST position vector in spacecraft body-fixed coordinate system (V-frame)

$$= [VE] \, \hat{R}_E \tag{3-6}$$

$\hat{R}_E$ = unit ST position vector in equatorial inertial coordinates (E-frame)

$[VE]$ = coordinate transformation matrix from the E-frame to the V-frame

$$= \begin{bmatrix} (q_1^2 - q_2^2 - q_3^2 + q_4^2) & 2(q_1 q_2 + q_3 q_4) & 2(q_1 q_3 - q_2 q_4) \\ 2(q_1 q_2 - q_3 q_4) & (-q_1^2 + q_2^2 - q_3^2 + q_4^2) & 2(q_3 q_4 + q_1 q_4) \\ 2(q_1 q_3 + q_2 q_4) & 2(q_2 q_3 - q_1 q_4) & (-q_1^2 - q_2^2 + q_3^2 + q_4^2) \end{bmatrix} \tag{3-7}$$

In Equation (3-7), q_1, q_2, q_3, and q_4 are the components of the inertial reference quaternion $\vec{q}$.

3.4 CALCULATION OF GEOMAGNETIC FIELD

The geomagnetic field to be computed by the STOCC can be modeled either by spherical harmonic expansions or by magnetic dipoles. The equations necessary for both models are presented in this subsection. A more complete discussion of the spherical harmonic expansion model can be found in Reference 3-3 and that of the magnetic dipole model, which is the model to be used onboard the ST, is given in References 3-1 and 3-4.

3.4.1 Spherical Harmonic Model

The geomagnetic field in the spacecraft body coordinate $\vec{B}$ can be obtained through the following transformation:

$$\vec{B} = [VE] \, [GE]^T \vec{B}_G \tag{3-8}$$
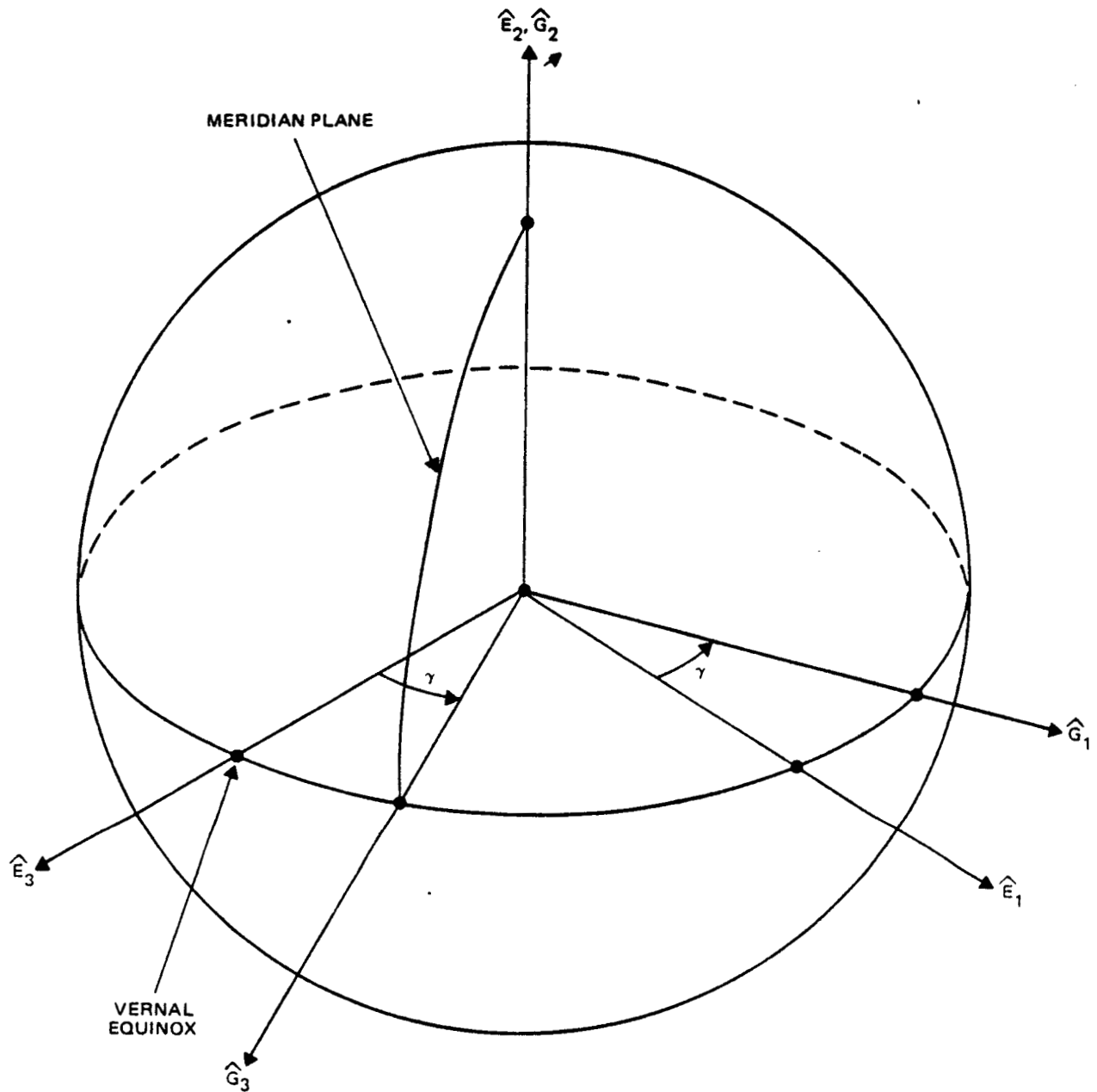
Figure 3-2. Coordinate System Definitions

where [VE] = transformation matrix from the equatorial inertial coordinate to the body-fixed coordinate as given by Equation (3-7)

[GE] = transformation matrix from the E-frame to the Earth-fixed coordinate system (G-frame) (see Figure 3-2)

$$= \begin{bmatrix} \cos\gamma & 0 & -\sin\gamma \\ 0 & 1 & 0 \\ \sin\gamma & 0 & \cos\gamma \end{bmatrix} \tag{3-9}$$

$$\gamma = \gamma_0 + \Omega_E t$$

γ_0 = angle from vernal equinox to prime meridian at time $t = 0$

Ω_E = Earth rotation rate

B_G = geomagnetic field vector expressed in G-frame

The magnetic field vector $\vec{B}_G$ can be expressed in terms of spherical harmonics by the following:

$$B_r = \sum_{n=1}^{k} \left(\frac{a}{r}\right)^{n+2} (n+1) \sum_{m=0}^{n} (g^{n,m} \cos m\phi + h^{n,m} \sin m\phi) \, P^{n,m}(\theta)$$

$$B_\theta = -\sum_{n=1}^{k} \left(\frac{a}{r}\right)^{n+2} \sum_{m=0}^{n} (g^{n,m} \cos m\phi + h^{n,m} \sin m\phi) \frac{\partial P^{n,m}(\theta)}{\partial \theta} \tag{3-10}$$

$$B_\phi = \frac{-1}{\sin\theta} \sum_{n=1}^{k} \left(\frac{a}{r}\right)^{n+2} \sum_{m=0}^{n} m \, (-g^{n,m} \sin m\phi + h^{n,m} \cos m\phi) \, P^{h,m}(\theta)$$

Here, B_r, B_θ, and B_ϕ are the radial (outward positive), coelevation (South positive), and azimuth (East positive) components of B_G, respectively. a is the equatorial radius of the Earth. r, θ, and ϕ are the geocentric distance, coelevation, and East longitude from Greenwich of the spacecraft position. $P^{n,m}$ are the Gauss-normalized associated Legendre polynomials, which can be obtained from the following recursion relations:

$$P^{0,0} = 1$$

$$P^{n,n} = \sin \theta \, P^{n-1,\,n-1}$$

$$P^{n,m} = \cos \theta \, P^{n-1,m} - K^{n,m} \, P^{n-2,m} \qquad (3\text{-}11)$$

$$K^{n,m} = \frac{(n-1)^2 - m^2}{(2n-1)(2n-3)}, \quad n > 1$$

$$K^{n,m} = 0, \qquad n = 1$$

The recursion relations for the partial derivatives of $P^{n,m}$ are given by

$$\frac{\partial P^{0,0}}{\partial \theta} = 0$$

$$\frac{\partial P^{n,n}}{\partial \theta} = (\sin \theta) \frac{\partial P^{n-1,\,n-1}}{\partial \theta} + (\cos \theta) \, P^{n-1,\,n-1} \qquad (3\text{-}12)$$

$$\frac{\partial P^{n,m}}{\partial \theta} = (\cos \theta) \frac{\partial P^{n-1,m}}{\partial \theta} - (\sin \theta) \, P^{n-1,m}$$

$$-K^{n,m} \frac{\partial P^{n-2,m}}{\partial \theta}$$

To reduce the computation time, the following recursion relations should be used for $\cos m\phi$ and $\sin m\phi$:

$$\cos m\phi = \cos\left[(m-1)\phi\right]\cos\phi - \sin\phi \sin\left[(m-1)\phi\right]$$

$$\sin m\phi = \sin\left[(m-1)\phi\right]\cos\phi + \sin\phi \cos\left[(m-1)\phi\right]$$

(3-13)

The constants $g^{n,m}$ and $h^{n,m}$ in Equation (3-10) are related to the Gaussian coefficients g_n^m and h_n^m by the following relations:

$$g^{n,m} \equiv S_{n,m}\, g_n^m$$

$$h^{n,m} \equiv S_{n,m}\, h_n^m$$

(3-14)

where $S_{n,m}$ can be calculated from the following recursion relations:

$$S_{0,0} = 1$$

$$S_{n,0} = S_{n-1,0}\left[\frac{2n-1}{n}\right], \qquad n \geq 1$$

$$S_{n,m} = S_{n,m-1}\sqrt{\frac{(n-m+1)\,(\delta_m^1 + 1)}{n+m}}, \, m \geq 1$$

(3-15)

In Equation (3-15), δ_m^1 is the Kronecker delta defined as $\delta_j^i = $ if $i = j$ and 0 otherwise.

The Gaussian coefficients g_n^m and h_n^m are determined empirically by a least-squares fit to measurements of the field. The coefficients for the International Geomagnetic Reference Field (IGRF) for epoch 1975 are given in Reference 3-3.

3.4.2 Magnetic Dipole Model

The magnetic dipole model used onboard the ST represents the geomagnetic field in the Earth-fixed coordinate frame, $\vec{B}_G$, by six magnetic dipoles. That is,

$$\vec{B}_G = \sum_{i=1}^{6} \frac{1}{|\vec{R}_i|^3} \left\{ -\vec{E}_{mi} + \frac{3}{|\vec{R}_i|^2} \left(\vec{R}_i \cdot \vec{E}_{mi} \right) \vec{R}_i \right\} \tag{3-16}$$

where
$$\vec{R}_i = \vec{R}_G - \vec{R}_{oi}$$
$$\vec{R}_G = [GE] \, RE$$
$\vec{R}_E$ = ST position vector in equatorial inertial coordinates
$\vec{R}_{oi}$ = position vector of the ith dipole
$\vec{E}_{mi}$ = dipole moment vectors of the ith dipole

In Equation (3-16), $\vec{R}_E$ is obtained from the spacecraft ephemeris computation. [GE] is the transformation matrix given in Equation (3-9), and $\vec{R}_{oi}$ and $\vec{E}_{mi}$ were determined by LMSC (Reference 3-4) to minimize the root-mean-square (rms) error in the magnetic field. It was concluded (Reference 3-1) that with this modeling, no update of the dipole data is necessary within the 15-year lifetime of the ST.

After $\vec{B}_G$ is obtained from Equation (3-16), the geomagnetic field in the ST body-fixed coordinate can be computed using Equation (3-8).

REFERENCES

3-1. Lockheed Missiles and Space Company, SE EM No. PCS-205, _Momentum Management Computations Performed by STOCC_, A. Wernli, July 1978

3-2. F. B. Hildebrand, _Introduction to Numerical Analysis_. New York: McGraw-Hill, Inc., 1956

3-3. Michael Plett, "Magnetic Field Models," _Spacecraft Attitude Determination and Control_. Dordrecht, Holland: D. Reidel, 1978

3-4. Lockheed Missiles and Space Company, PCS-102, _Onboard Implementation of the Space Telescope Momentum Management System_, A. Wernli, January 1978

SECTION 4 - OPERATIONAL IMPACT OF ONBOARD CONTROL LAWS

4.1 APPLICABILITY OF THE CP AND ME CONTROL LAWS

The primary requirement of the momentum management control law is to main-
tain speeds of the reaction wheels below 10 hertz (References 4-1, 4-2, and 4-3).
The performance of three control laws, including both the CP and ME laws, has
been evaluated for various inertially fixed attitudes in a series of 24-hour simu-
lations (Reference 4-2). In another study (Reference 4-4), the ME control law
was evaluated during simulated slew maneuvers. A comparison of the ME law
and the modified CP law during maneuvers is given in Reference 4-5. The re-
sults of these studies are summarized below.

In the first investigation, gravity-gradient torques were calculated assuming
that the ST maintained an inertially fixed attitude. Nominal ST orbital elements
and a simple dipole model of the geomagnetic field were used. Table 4-1 lists
peak wheel speeds for the "worst case" condition, i.e., the V1-axis pointing
45 degrees out of the orbit plane.[1] These data were obtained with a magnetic
dipole moment limit of 1800 ampere-meters^2 (A-m^2) per coil. For the ME
simulations, a desaturation period of 600 seconds and an update period of
200 seconds were used.

In the second investigation, slew maneuvers were simulated to evaluate the per-
formance of the ME law. Slew rates of 0.15 degree per second were assumed.
For each maneuver a single desaturation period, consisting of a lead time, the
maneuver, and a lag time, was employed. Conclusions were reached about two
functions: the minimum lead and lag time required to achieve the desired angu-
lar momentum and peak reaction wheel speeds during the lead and lag times.

---

[1] These data do not necessarily represent the worst cases. Increases in reac-
tion wheel speed of up to 20 percent were noted for smaller angles.

Table 4-1. Comparison of Peak Reaction Wheel Speeds for
the CP and ME Control Laws (Reference 4-2)

Control Law	Peak Reaction Wheel Speed (Hz)	
	CP	ME
Normal Operation	10.3	7.8
Detected Coil Failure	11	8.6
Undetected Coil Failure	14.8	10.3
Undetected Tachometer Failure	27	21
Detected RW Failure	18	13.5
Undetected RW Failure	11	13.5

It was found that the minimum required lead and lag times vary from zero to some maximum value depending on the initial attitude and the direction of the slew. The maximum value is nearly independent of the size of the slew angle for slews larger than 30 degrees. Worst case maneuvers, i.e., those requiring the longest lead and lag times, were confined to a set of unfavorable orbital track segments within the following approximate ranges: longitudes between 150 and 300 degrees when the spacecraft latitude is decreasing or longitudes between 240 and 340 degrees when the spacecraft latitude is increasing. Table 4-2 compares the maximum lead and lag times required for favorable and unfavorable orbital track segments for different magnetic torquer conditions. Only a small percentage of the cases studied required the maximum times noted in Table 4-2.

Peak reaction wheel speeds during each lead and lag time were noted. The peak reaction wheel speed appears to be insensitive to the length of the lead and lag time, but does depend on the following parameters: the amount of angular momentum required to be dumped, $\vec{H}_D$; the relative directions of $\vec{H}_D$ and the geomagnetic field as seen by the ST, $\vec{B}$; and the change in $\vec{B}$ during the maneuver. The reaction wheel speed limit of 10 hertz was exceeded in 5 percent of the maneuvers when four reaction wheels were operational and in 15 percent of the maneuvers when only three reaction wheels were operational. When all four reaction wheels were available, excessive speeds were confined to the unfavorable orbit track segments defined above; however, only a small fraction of the maneuvers in the unfavorable regions result in excessive speeds. No suitable parameters were found in Reference 4-4 for predicting which maneuvers would yield excessive reaction wheel speeds, and it was concluded that simulations were required to identify such maneuvers.

The performances of the modified CP law (Section 2.2.1) and the ME law (with and without lead and lag times) are directly compared in Reference 4-5. Each

Table 4-2. Maximum Lead and Lag Times

Orbit Track Segment	Lead and Lag Times			
	2800 A-m^2 Mag. Dipole Limit		4000 A-m^2 Mag. Dipole Limit	
	4 Torquers	3 Torquers	4 Torquers	3 Torquers
Favorable	500 sec	700 sec	350 sec	500 sec
Unfavorable	900 sec	1200 sec	700 sec	900 sec

of 14 maneuvers was simulated using each of the three laws. Slew angles varied from 30 to 180 degrees. More than half of these maneuvers were designated as "difficult" cases based on the type of maneuver and orbit track segment. The performance of the ME law without lead and lag times was generally inferior to that of the other methods and will not be discussed here.

Performance of the control laws was evaluated on the basis of two criteria: the number of cases in which the reaction wheel speeds exceeded 10 hertz outside of the maneuver period and the maximum time required to settle below the 10-hertz limit. Maneuvers were simulated both assuming that all four reaction wheels were operational and assuming that one RWA was disabled. Also, the tests were repeated with estimation errors, i.e., a mismatch between environmental and model representations of the gravity-gradient torque and geomagnetic field. ($\vec{T}_{GG}$ was overestimated by 10 percent and $\vec{B}$ allowed to vary up to 40 percent.) The results of the study are presented in Table 4-3.

For tests in which all the RWAs are operational, the performance of the ME law appears to be superior. ME law failures, i.e., maneuvers resulting in excessive reaction wheel speeds, were a subset of the CP law failures. In four of these cases the SAA was encountered during the maneuver. Momentum management is difficult during SAA passage because the geomagnetic field has a low magnitude and only small variations in direction. Introduction of estimation errors had a greater effect on the performance of the ME law than on that of the CP law; however, use of the ME law still resulted in fewer failures and significantly shorter times required to settle below the reaction wheel speed limit.

For tests in which only three RWAs were operational, more failures were observed for both laws and the ME law failed nearly as often as the CP law. The CP law, however, requires considerably more time to settle below the 10-hertz limit without estimation errors. The introduction of estimation errors resulted in cases where the maximum reaction wheel speed never dropped below this limit. While the ME law failed as often as the CP law under these conditions, the

Table 4-3. Performance of the Modified CP Law and the ME Law
With Lead and Lag Times for 14 Identical Maneuvers

Conditions	Number of Cases Exceeding 10-hertz Reaction Wheel Speed		Maximum Time Required to Settle Below 10-hertz Reaction Wheel Speed (seconds)	
	CP	ME	CP	ME
Four RWAs Operational				
No Estimation Errors	6	3	2500	1300
With Estimation Errors	6	5	2500	1450
Three RWAs Operational				
No Estimation Errors	9	7[a]	5600	1400
With Estimation Errors	9	9	∞[b]	∞[b]

[a] This includes cases where the 10-hertz limit was exceeded during lead time.

[b] A steady-state condition of reaction wheel speed greater than 10-hertz was obtained.

CP law resulted in higher maximum reaction wheel speeds. During the maneuver, the maximum speed exceeded 50 hertz in three CP law cases and two ME law cases. Because 50 hertz is the maximum speed that a reaction wheel can achieve and still produce maximum torque output, these maneuvers are unattainable.

Tentative conclusions may be drawn from the results of the three studies reviewed above. They include the following:

- For inertially fixed attitudes, both the CP and ME laws appear to be adequate for maintaining reaction wheel speeds below the 10-hertz limit during normal operation. Both laws fail or are only marginally successful in various cases of onboard hardware failure. In all but one case the ME control law is superior.

- Both laws result in excessive wheel speeds following certain difficult maneuvers. (The ME law can also fail in the lead time before a maneuver.) The ME law fails in approximately 5 percent of maneuvers during normal operation and 10 percent of maneuvers with a reaction wheel failure. The CP law fails more frequently. Difficult maneuvers occur in a limited range of orbit track segments; however, many maneuvers in these ranges are satisfactory. At present, the only method known to distinguish the difficult maneuvers is computer simulation of the maneuvers.

- Difficult maneuvers require settling times of up to 1400 seconds for the ME law and 5600 seconds for the CP law with onboard hardware failure; if estimation errors are included in the simulation, steady-state reaction wheel speeds greater than 10 hertz sometimes result for both laws. Under extreme conditions, some maneuvers are impossible because reaction wheel speeds in excess of 50 hertz are reached.

In general, the performance of the ME law is superior. If the CP law were implemented onboard the ST, the ME law (or an equivalent technique) would still be required for some worst case targets, difficult maneuvers, and in the event of hardware failure. It would be necessary to identify such targets and maneuvers at the STOCC prior to uplink to the ST and to inform the onboard computer as to which control law to use at each target. In a few cases the ME law is inadequate also. Such situations must be identified and avoided.

4.2 IMPACT ON ROUTINE OPERATIONS

The CP control law can be entirely implemented onboard the ST. No computation at the STOCC is required to support the CP law, except the generation of commands to disable a reaction wheel or magnetic torquing coil and to turn the control law on and off.

The ME control law requires considerably more software to support its implementation. As explained in Section 3, ME ground support hardware must generate a set of Fourier coefficients representing the nominal momentum profile for each inertial target. The Fourier coefficients are calculated by numerical integration of the magnetic and gravity-gradient torques over half an orbit in N steps where the recommended value of N is 5. The numerical integration requires the calculation of $\vec{T}_M$, $\vec{T}_{GG}$, and $\vec{B}$ at 4N (20) points. The calculation of $\vec{T}_M$ involves two additional numerical integrations. Computer storage and execution time required for ground support of the ME control law can be estimated from execution of the Profile program (Reference 4-6). The Profile program has been used to study momentum management for the Solar Maximum Mission (SMM). Profile calculates $\vec{B}$ and several disturbance torques, including $\vec{T}_{GG}$. Execution requires 230K bytes of storage on the GSFC IBM S/360-95 computer. Calculation of all parameters for a 2-day interval in steps of 3 minutes (a total of 960 steps) requires approximately 0.4 minute of of CPU time on the same computer. It is estimated that the numerical integrations required for the ST application would take no longer to perform

4-8

than the calculation of the additional disturbance torques now performed by Profile.

Therefore, it is estimated that the 20 steps required for each ST target could be performed in approximately 0.01 minute on the same computer. Processing 20 targets per day would require 0.2 minute of CPU time on the S/360-95 computer or 1 to 2 minutes in the high-speed core of the GSFC IBM S/360-65 computer.

Guide star selection and target sequencing by the STOCC are expected to require significantly more computational support than momentum management. For the High Energy Astronomy Observatory-2, guide star selection and target sequencing are performed by the Detailed Observing Program (DOP) (Reference 4-7). The DOP is executed in the high-speed core of the GSFC IBM S/360-65 computer and requires 10 to 20 minutes of CPU daily. Therefore, guide star selection and target sequencing are expected to require an order of magnitude more CPU time than computation of the Fourier coefficients for the nominal momentum profiles.

The lengths of the lead and lag times also must be supplied to the onboard computer (see Section 2.3.2.1). Computation of the minimum lead and lag times would require simulation of every maneuver. Alternatively, maximum times could be determined for various types of maneuvers as done in Tables 4-2 and 4-3. The type of maneuver could then be determined and lead and lag times could be assigned with negligible impact to STOCC operations. Peak reaction wheel speeds are not affected by lead and lag time lengths; however, assignment of maximum lead and lag times might require longer dwell times at targets and thus have scientific impact.

As noted in Section 4.1, the CP law fails and, less frequently, the ME law fails for some targets, maneuvers, and hardware failures. Presently, simulations are required to identify such cases. It is hoped that continued study will result

in parameterization of these events so that simulations will not be necessary for identifications. Simulation of maneuvers can be expected to have much larger computational impact than the calculation of nominal momentum profiles discussed above. Because ME failures appear to be a subset of CP failures, perhaps the ME law should be implemented for all sequences with a high probability of failure. Then only simulation of the ME law would be required to identify unfeasible sequences.

4.3 IMPACT ON SCIENTIFIC PROGRAM

The primary impact of momentum management on the ST scientific program is that some targets, maneuvers, or situations may not be feasible because of failure of the control law chosen to limit reaction wheel speeds. This subsection reviews momentum management constraints on the scheduling of normal targets as well as targets of opportunity, serendipity targets, and target branching. (See Reference 4-8 for descriptions of these special types of targets.)

For inertial pointing during normal operation, the CP law appears to be adequate for most targets and the ME law appears to be feasible for all targets. Thus, there are no areas of the celestial sphere which are inaccessible during normal operations. For various onboard hardware failures, both control laws fail for some targets and orbit track segments. If vibrations in the ST resulting from excessive reaction wheel speed fail to damp out quickly, it is possible that certain regions of the sky (perhaps bands parallel to the ST orbital plane) would be permanently unobservable by the ST.

The ME control law also fails in approximately 5 percent of normal maneuvers and in approximately 15 percent of maneuvers with only three operational RWAs. If it is necessary to avoid such maneuvers, then certain target sequences would be impossible. When combined with other restrictions because of bright object avoidance, occultations, etc., momentum management restrictions on target sequences may cause delays in completing observing programs, especially those requiring observations at specific times such as variable star studies.

Targets of opportunity are those which pertain to unpredictable, short-lived astronomical events such as novae or transient solar system phenomena. The STOCC should be able to schedule such targets within a few hours of notification of the discovery. The scheduling system should be capable of processing approximately one target of opportunity per week.

Scheduling targets of opportunity will be complicated by momentum management considerations. The STOCC must generate a new target sequence, which includes the target of opportunity, to replace the target sequence in effect. If the ME control law is implemented, lead and lag times must be determined for the new maneuvers and nominal momentum profiles must be calculated for the targets. For either control law it may be necessary to screen the new maneuvers against the control law failures discussed above. Maneuver to the target might be delayed until a favorable orbit track segment occurs. If determination of lead and lag times and screening of maneuvers require computer simulations, generation of the target sequence may be slowed, causing additional scheduling delays. Because of the transient nature of targets of opportunity, any delay in observation may have major scientific impact. Also, for some types of hardware failure, inertial pointing at the target may violate the reaction wheel speed limit. Such a control law failure may make observation of the event impossible.

Serendipity targets are those that happen to be available to a second scientific instrument (SI) during observation of a normal target by the primary SI. In particular, the wide field camera (WFC) frequently can be utilized while the normal observations proceed. The observer of serendipity targets has no control over attitude or exposure time. The principal constraint on serendipity mode observations is availability of power. Because serendipity targets are observed simultaneously with normal targets, momentum management procedures impose no additional constraints on their execution.

Branching refers to an option in real-time operations whereby alternative observing sequences are scheduled and the experimenter chooses between them

4-11

prior to the time of observation. One sequence of targets is uplinked to the ST and that sequence is executed unless the experimenter chooses the alternative sequence. The experimenter must make his/her choice in time to uplink the new commands before the maneuver. Both series of commands must be generated in advance. Thus, any calculations required for momentum management must be repeated for each sequence. These calculations include screening of targets and maneuvers and, for the ME control law, computation of the nominal momentum profile and determination of lead and lag times. If simulations are required, the amount of computation may limit the use of the branching technique.

4.4 ESTIMATION OF REQUIRED RESOURCES

Required ground support for implementation of the ME control law includes generation of the nominal momentum profile and lengths of the lead and lag times. Screening of targets and maneuvers appears to be necessary for the implementation of either the CP law or the ME law. Because the CP law can be implemented entirely onboard the ST, no additional software and hardware resources are required on the ground for its support.

Calculation of nominal momentum profiles would require computer resources similar to those needed to execute program Profile, which is described in Reference 4-6. Many of the Profile subprograms, which are written in FORTRAN, are standard utilities in use at GSFC.

Computer simulations may be required for the calculation of ME law lead and lag times and the screening of targets and maneuvers. A rough estimate of the resources required for such simulations may be obtained from a comparison with the High Energy Astronomy Observatory-2 (HEAO-2) Attitude Control Simulator (HACS) (Reference 4-9). HEAO-2 and ST both employ onboard computers, gyros, star trackers, and reaction wheels for attitude control. The HEAO-2 HACS simulates the operation of all onboard hardware necessary for

attitude control and generates corresponding output telemetry. Much of the code in HACS, which is written in FORTRAN, is unique to the HEAO application.

When HACS is executed on the GSFC IBM S/360-95 computer with the least time-consuming option (i.e., no star trackers and minimal output), HACS can perform 60 integration steps per CPU second. For HEAO applications, the step size is 0.32 second. Because the step size required for ST momentum management applications is unknown, no estimate of the total time requirement is possible.

Execution of HACS nominally requires 410K bytes of storage at the GSFC IBM S/360-95 computer. Reduction of the program to perform only functions of the type required for ST momentum management could significatly reduce this core requirement.

Analaysis of the descriptions of Profile and HACS in References 4-6 and 4-9 indicates that development and operation of a simulator of ST momentum management may require considerably more resources than development and operation of a program to calculate only nominal momentum profiles.

REFERENCES

4-1. A. Wernli, "Minimization of Reaction Wheel Momentum Storage with Magnetic Torquers," J. Astronautical Sciences, vol. 26, no. 3, p. 257, July-September 1978

4-2. Lockheed Missiles and Space Company, LMSC-HREC TM D496086, Reaction Wheel Speed Minimization through Magnetic Desaturation, A. Wernli, November 1976

4-3. --, SE-03, Section H, Space Telescope Project, Support Systems Module, Appendix 3, April 1979

4-4. --, SE EM No. PCS-105A, Momentum Management with ME Law during Slew Maneuvers, A. Wernli, August 1978

4-5. Bendix Corporation, ST-2044 Rev A, Comparison Study of the Minimum Energy and Cross-Product Momentum Desaturation Laws, A. K. Nakashima, November 1978

4-6. Computer Sciences Corporation, CSC/SD-79/6080, Solar Maximum Mission (SMM) Truth Model Attitude Simulator Algorithm Description and Operating Guide, F. E. Baginski et al., June 1979

4-7. --, CSC/TM-79/6125, Program Overview and Functional Description of High Energy Astronomy Observatory Satellite-2 (HEAO-2) Detailed Observing Program (DOP) Target Sequencer, A. N. Suri, October 1979

4-8. Lockheed Missiles and Space Company, LMSC 4171847A, ST Mission Operations Requirements, DR OP-01, volume III, August 1979

4-9. Computer Sciences Corporation, CSC/TM-78/6115, High Energy Astronomy Observatory-B (HEAO-B) Attitude Control Simulator (HACS) User's Guide, C. R. Sturch, July 1978

SECTION 5 - PHYSICAL INTERPRETATION OF CONTROL LAWS AND ALTERNATIVE TECHNIQUES

5.1 INTRODUCTION

The purpose of this section is to provide physical interpretation of the control laws to better understand and compare their performance, to help improve the current techniques, and to develop new techniques. In general, a desaturation control law is a method of reducing the build-up of spacecraft momentum due to external environmental torques by generating a magnetic torque resulting from the interaction between the geomagnetic field and the commanded magnetic torquers situated on the spacecraft.

Each control law can in general be put into one of two main categories, depending on its type of control--closed loop or open loop. In a closed-loop control law, the magnetic dipole command is updated using instantaneous measurements with the intent to achieve a desired torque at each update time. In an open-loop control law, the magnetic dipole command is updated using predicted information with the intent to achieve a desired momentum at the end of each update period. Within each control type, control laws can be further characterized by their special criteria or constraints. These criteria or constraints are independent of the control type. That is, every control law can be either closed loop or open loop regardless of which quantity is minimized or which constraint is undertaken. Thus, to specify a control law clearly, it is necessary to specify not only criteria or constraints but also the control type.

In principle, a "minimum energy" law can be either a closed-loop law or an open-loop law depending on how the magnetic dipole command is generated. The traditional way of using "CP law" to represent a closed-loop law and "ME

law" to represent an open-loop law is confusing from a physical point of view. Open-loop laws, for example, can be derived based on simplicity. Either the magnetic moment or the torquer commands could be held constant during the desaturation intervals to produce the same end momentum conditions as an open-loop minimum energy law which keeps the direction of the desired torque constant. Actually, the ME law implemented for ST is an open-loop control law that minimizes the total energy consumed by the magnetic torquers during the desaturation period. The CP law implemented for ST is a closed-loop control law that minimizes the magnitude of the instantaneous reaction wheel speed.

In the remainder of this section, these two ST control laws will be referred to as the "current ME law" and the "current CP law" to distinguish them from other alternative control laws that carry similar minimization criteria.

Section 5.2 describes the control laws in general. Emphasis is given to the physical interpretations of the control laws, their similarities, differences, merits, and drawbacks. Section 5.3 summarizes the current control laws implemented for ST and discusses their problem areas. Section 5.4 presents alternative techniques for both inertial targets and maneuvers based on our physical understanding of the control laws. The new techniques are believed to have some advantages over the current ST implementations and may resolve several of the problems associated with the current laws.

5.2 PHYSICAL INTERPRETATION AND GENERAL DISCUSSION

5.2.1 PHYSICAL INTERPRETATION

With some rearrangement, the current control laws can be described by a simple set of equations given in Table 5-1. In the table, all quantities are put into comparable forms to enable an easy comparison between a closed-loop and an open-loop control law and between control laws with different minimization criteria. The physical meaning of each of the quantities listed in Table 5-1 is described below.

In the table, $\vec{T}_D$ is a desired torque, which is the torque a closed-loop control law is attempting to achieve momentarily through the interaction between the magnetic torquers and the geomagnetic field. Here $\vec{H}_D$, which is defined for open-loop control laws only, is the integration of a desired torque over a period of time (called the desaturation period). Physically, $\vec{H}_D$ is the desired momentum an open-loop control law attempts to achieve over the desaturation period through the interaction between the magnetic torquers and the geomagnetic field. Thus, the fundamental difference between the open-loop and the closed-loop control laws is that the former attempts to achieve $\vec{T}_D$ momentarily, whereas the latter attempts to achieve $\vec{H}_D$ over a desaturation period. The determination of $\vec{T}_D$ and $\vec{H}_D$ is briefly discussed below. For all control laws based on Equation (2-4), $\vec{T}_D$ is obtained by replacing $\vec{T}_M$ with $\vec{T}_D$ in the equation. That is,

$$\vec{T}_D = \dot{\vec{H}}_T - \vec{T}_{GG} \qquad (5\text{-}1)$$

where $\vec{H}_T$ is the total system momentum that equals the reaction wheel momentum $\vec{H}_{RW}$ at inertial attitudes. For a

Table 5-1. Summary of Equations for Current Control Laws

	CURRENT CP LAW (CLOSED-LOOP MINIMUM WHEEL SPEED LAW)	CURRENT ME LAW (OPEN-LOOP MINIMUM ENERGY LAW)
DESIRED TORQUE	$\vec{T}_D$	
DESIRED MOMENTUM	NOT APPLICABLE	$\vec{H}_D = \int_{t_i}^{t_f} \vec{T}_D\, dt$
WEIGHTING MATRIX	A	
COSTATE VECTOR	$\vec{P} = (\tilde{B}^T A A^T \tilde{B})^{-1} \vec{T}_D$	$\vec{P} = \left[\int_{t_i}^{t_f} \tilde{B}^T A A^T \tilde{B}\, dt\right]^{-1} \vec{H}_D$
SYSTEM MAGNETIC DIPOLE MOMENT	$\vec{\mu}_M = A A^T \tilde{B} \vec{P}$	$\vec{\mu}_M = A A^T \tilde{B} \vec{P}$
MAGNETIC TORQUE	$\vec{T}_M = \vec{\mu}_M \times \vec{B}$	
COMMANDED MAGNETIC DIPOLE MOMENT	$\vec{\mu}_T = M^T (MM^T)^{-1} \vec{\mu}_M$	

7081/80

5-4

closed-loop control law, $\vec{H}_T$ in Equation (5-1) is usually replaced by $-K_M(\vec{H}_T + \vec{H}_B)$, where K_M is a positive constant called the magnetic gain and $\vec{H}_B$ is a bias vector that is added to $\vec{H}_T$ to keep the reaction wheel center speed at zero. For an open-loop control law, Equation (5-1) is integrated over the desaturation period to give the desired momentum, $\vec{H}_D$. That is,

$$\vec{H}_D = \int_{t_i}^{t_f} \vec{T}_D \, dt$$

$$(5-2)$$

$$= \vec{H}_T(t_f) - \vec{H}_T(t_i) - \int_{t_i}^{t_f} \vec{T}_{GG} \, dt$$

where $\vec{H}_T(t_f)$ is the desired total momentum at the end of the desaturation period and $\vec{H}_T(t_i)$ is the measured total momentum at the start of the desaturation period. The length of the desaturation period controls the magnitude and direction of $\vec{H}_D$. Nominally, the desaturation period is set at half an orbital period to include the major variations in the geomagnetic field and to be compatible with the period of the gravity-gradient disturbances so that only the nonperiodic portion of the accumulated gravity-gradient momentum is dumped.

The weighting matrix A of Table 5-1 is determined by the minimization criteria. A is the magnetic coil mounting matrix, M, in the current ME law to minimize the energy consumption and is the wheel mounting matrix, W, in the current CP law to minimize the reaction wheel speed. In the following discussion, to simplify the physical interpretations, an orthogonal system with A equal to the identity matrix will be assumed.

The costate vector $\vec{P}$ is defined differently for the two control laws due to the different control types.[1] For a closed-loop control law, $\vec{P}$ is the desired torque weighted by $|\vec{B}|^{-2}$, where $\vec{B}$ is the geomagnetic field. For an open-loop control law, $\vec{P}$ is the desired momentum weighted by both the magnitude and the direction of the geomagnetic field over the desaturation period. The physical meaning of $\vec{P}$ for an open-loop control law is illustrated in Figure 5-1 with the assumption that the magnitude of $\vec{B}$ is constant in time. As shown in Figure 5-1, $\vec{P}$ is a fictitious torque whose component along the direction normal to the instantaneous geomagnetic field is the instantaneous magnetic torque, $\vec{T}_M$, generated by the torquers. The integration of $\vec{T}_M$ over the desaturation period is equal to $\vec{H}_D$. The costate vector $\vec{P}$ in an open-loop control law is analogous to the desired torque $\vec{T}_D$ in a closed-loop control law after being properly weighted. Figure 5-1 also illustrates the significance of the desaturation period for an open-loop control law. Three cases covering different desaturation periods are shown in Figure 5-1. When the desaturation period is very short, as illustrated in Figure 5-1(a), $\vec{P}$ approaches infinity due to the near-singular condition. In this case, the magnetic torquers are given poorly defined commands with the result that the magnetic torques generated may go through an undesirable path before the desired momentum is achieved.

----

[1] In the derivations of the original CP and ME laws in Section 2, the costate vector, $\vec{P}$, was defined only for the ME law. However, an analogous definition, stated in Table 5-1, may be introduced for the CP law. Use of this definition of $\vec{P}$ clarifies the similarities between the two laws and facilitates the physical understanding of the $\vec{P}$ defined in the ME law.

(c) $t_1 + t_2 + t_3 + t_4$
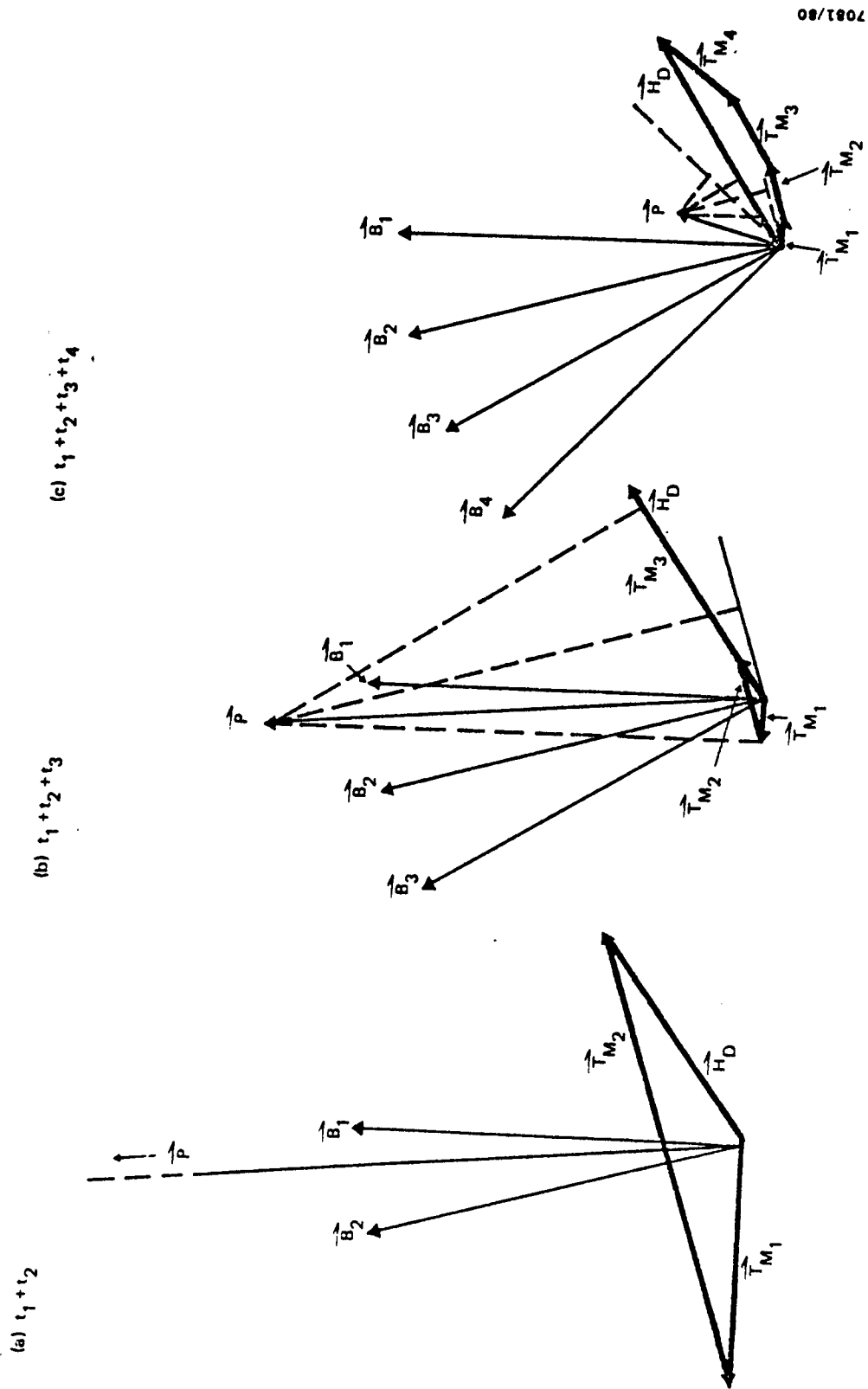
(b) $t_1 + t_2 + t_3$

(a) $t_1 + t_2$

Figure 5-1. Physical Interpretation of the Costate Vector in an Open-Loop Control Law

This is shown in Figure 5-1(a), where the magnetic torque $\vec{T}_{M_1}$ is along a direction almost opposite to the direction of the desired momentum $\vec{H}_D$. This can cause a very high reaction wheel speed at the end of t_1, which is certainly undesirable. Thus, an open-loop control law operated under very short desaturation periods can sometimes lead to serious consequences. As the desaturation period increases as shown in Figure 5-1(b) and (c), the costate vector $\vec{P}$ becomes better defined and the path of the magnetic torques becomes closer to the desired momentum.

The system magnetic dipole moment, $\vec{\mu}_M$, is the magnetic dipole moment (defined in the spacecraft body coordinate system) that is required to generate the desired magnetic torques. The magnetic torque $\vec{T}_M$ is the actual instantaneous magnetic torque generated from the interaction between the magnetic torquers and the geomagnetic field. The magnitude and direction of $\vec{T}_M$ are as follows. For a closed-loop control law, $\vec{T}_M$ is the component of $\vec{T}_D$ which is normal to $\vec{B}$. This component is the best torque that can be achieved under the condition that $\vec{T}_M$ must be perpendicular to $\vec{B}$, although ideally it would be desirable to generate a $\vec{T}_M$ that equals $\vec{T}_D$. When the weighting matrix A is different from the identity, the magnitude and direction of $\vec{T}_M$ differ slightly from those described above. For an open-loop control law, $\vec{T}_M$ is also perpendicular to $\vec{B}$ at any moment. However, $\vec{T}_M$ also satisfies the condition that its integrated effect over the desaturation period equals the desired momentum, $\vec{H}_D$. That is, $\vec{T}_M$ satisfies the condition that

$$\int_{t_i}^{t_f} \vec{T}_M \, dt = \vec{H}_D \qquad (5-3)$$
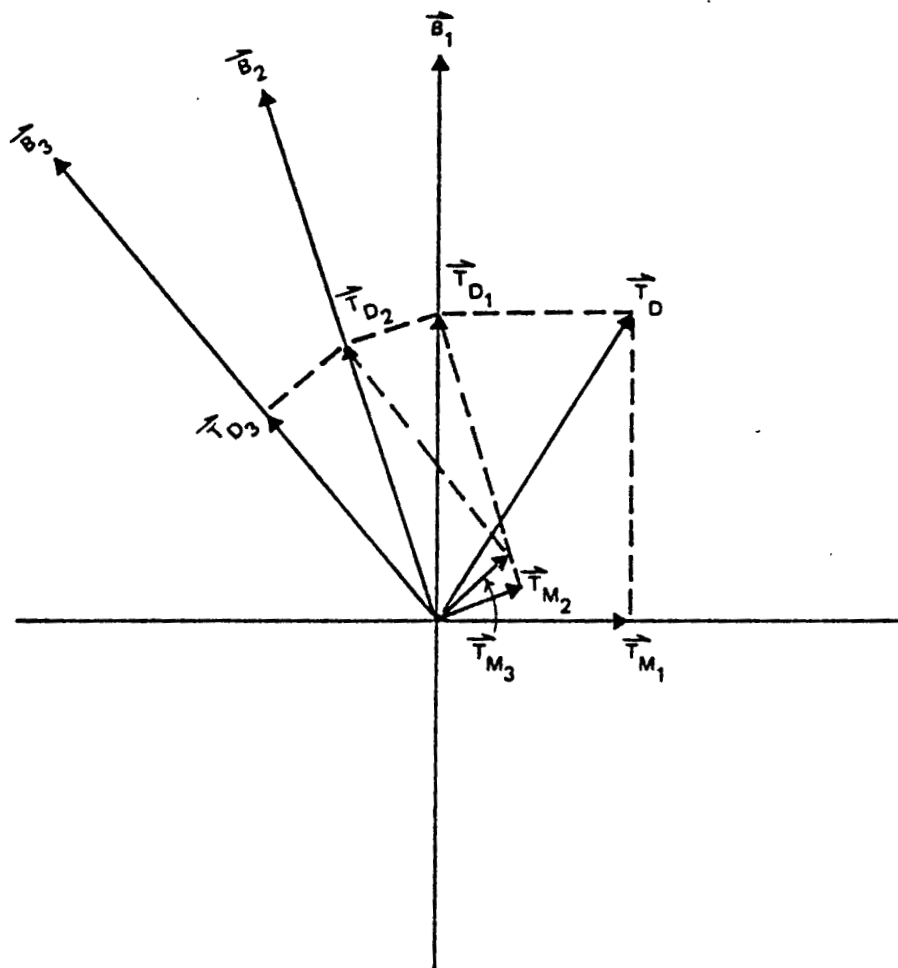
Figure 5-2. Geometrical Variations of the Desired
Torque for a Closed-Loop Control Law

This indicates that although the desired torques cannot always be generated momentarily, the desired momentum can usually be generated over a period of time, taking advantage of the variations in the geomagnetic field. This forms one major advantage of an open-loop control law over the closed-loop control law.
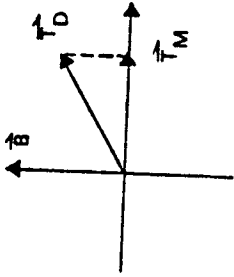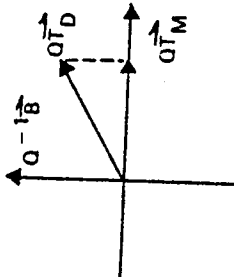
The last item in Table 5-1 is the commanded magnetic dipole moment $\vec{\mu}_T$. The components of $\vec{\mu}_T$ give the actual dipole moment required by each of the magnetic torquers to generate the magnetic torque $\vec{T}_M$, and $\vec{\mu}_T$ is the final output of a control law sent to the magnetic torquers.

The weighting matrix A defined in Table 5-1 is controlled by the minimization criteria of the control laws. The simplest control law minimizes the deviation between $\vec{T}_D$ and $\vec{T}_M$ in the body coordinates (MTD). The current CP law provides minimization of reaction wheel speeds (MWS) through use of reaction wheel mounting matrix W. The physical interpretations of $\vec{T}_M$ for these two laws are compared in Table 5-2.

5.2.2 COMPARISONS AND MODIFICATIONS

Both the closed-loop and the open-loop control laws have their merits and drawbacks. The greatest problem of a closed-loop law is that it attempts to achieve a desired torque momentarily, which is for all practical purposes impossible. As a result, it produces a magnetic torque that is the component of $\vec{T}_D$ normal to the geomagnetic field, which may be a small fraction of the total. This process also effectively projects the resultant torque into the direction of the geomagnetic field, which is an unfavorable direction for further reduction of the momentum. This situation is illustrated in Figure 5-2. Apparently a great deal of energy is wasted in changing the direction rather than reducing the magnitude of the momentum. Furthermore, the

Table 5-2. Physical Interpretation of $\vec{T}_M$ for Different Minimization Criteria

MINIMIZATION CRITERION	WEIGHTING MATRIX A	PHYSICAL INTERPRETATION OF $\vec{T}_M$
MINIMUM TORQUE DEVIATION (MTD)	$A = I$	$\vec{T}_M$ = THE COMPONENT OF $\vec{T}_D$ NORMAL TO $\vec{B}$
MINIMUM WHEEL SPEED (MWS)	$A = W = \begin{bmatrix} a & -a & a & -a \\ -b & b & b & -b \\ -b & -b & b & b \end{bmatrix}$ WHERE $a = \text{SIN } 20°$ $b = \frac{1}{\sqrt{2}} \text{COS } 20°$	$Q\vec{T}_M$ = THE COMPONENT OF $Q\vec{T}_D$ NORMAL TO $Q^{-1}\vec{B}$ WHERE $Q^2 = \begin{bmatrix} \frac{b^2}{a^2} & 0 & 0 \\ 0 & 1 & 0 \\ 0 & 0 & 1 \end{bmatrix} = 4b^2 (WW^T)^{-1}$

closed-loop control law attempts to always reduce the same
fraction of the total momentum as controlled by the magnetic
gain K_M, regardless of the variation in geometry. This is
not efficient, because the law should attempt to dump more
momentum when the geometry is favorable and less momentum at
an unfavorable geometry. In addition, the closed-loop con-
trol laws attempt to dump both the periodic and the nonperi-
odic gravity-gradient momenta, while only the nonperiodic
portion needs to be dumped in many applications. These
problems associated with the closed-loop control laws are
eliminated in the open-loop control laws, because the open-
loop control laws look at the situation ahead of time to
take advantage of the variations in geometry to dump the
proper amount of momentum at the proper time. Thus, at the
end of the desaturation period, the desired amount of momen-
tum will be generated from the torquers.

The open-loop control laws are ideal if actual performance
is exactly as predicted. However, in case of modeling er-
rors or undetected failure conditions, reality can be very
different from the prediction. This difference will not be
known until the end of the desaturation period, which may be
too late for correction. To resolve this potential problem,
a "modified open-loop control law" was suggested for ST that
uses the half-orbit desaturation period to compute the nomi-
nal momentum profile $\vec{H}_{NOM}$ (refer to Section 3) and then
uses $\vec{H}_{NOM}$ as the targeting momentum, $\vec{H}_T(t_f)$ of Equa-
tion (5-2), in computing $\vec{H}_D$ when a much shorter desatura-
tion period is used. With this modification, the advantages
of the open-loop control laws are kept by forcing the system
momentum to follow the same time variation it would follow
if a half-orbit desaturation period were used under nominal
situations. At the same time, the disadvantage of the
open-loop control laws is reduced by decreasing the duration

of the desaturation period and increasing the updating frequency so that the actual system momentum can be measured at a much higher frequency, and the deviation between the reality and the prediction can be included in $\vec{H}_D$ and corrected for at this new frequency.

In principle, with a precomputed $\vec{H}_{NOM}$, the shorter the update period the better, if undetected failure conditions exist. However, as discussed in Section 5.2.1, making the desaturation period of an open-loop control law arbitrarily short may cause the costate vector $\vec{P}$ to be ill defined and result in very undesirable momentum before the desired momentum is achieved. For this reason, a 600-second desaturation period with a 200-second updating frequency was recommended in the current momentum management implementation for ST. However, if instead of using an open-loop control law at a reduced desaturation period, a closed-loop control law is used with the precomputed $\vec{H}_{NOM}$, the problem of determining $\vec{P}$ will no longer exist. In this "mixed-mode control law," the updating frequency of commanding the magnetic torquers can be reduced to the frequency of the closed-loop control laws, which is approximately 50 seconds for ST. The fundamental concept of a mixed-mode law is to generate an instantaneous desired torque as in a closed-loop law, but to derive this torque from the expected momentum profile of an open-loop law. An approximation of Equation (5-1), which is a basic relationship of the current laws, can be used to generate such a desired torque, i.e.,

$$\vec{T}_D = \frac{1}{\Delta t} [\vec{H}_{NOM}(t + \Delta t) - \vec{H}_T(t)] - \vec{T}_{GG}(t) \qquad (5-4)$$

where Δt is a small time interval[1] during which $\vec{T}_{GG}$ does not change significantly and $\vec{H}_{NOM}$ is the nominal momentum profile computed previously based upon an open-loop control law with a half-orbit desaturation period. The desired torque so determined is always nearly perpendicular to the instantaneous geomagnetic field because $\vec{H}_{NOM}$ is computed from the nominal magnetic torques, which are momentarily perpendicular to $\vec{B}$. This mixed-mode control law, which is a closed-loop control law operated with an open-loop $\vec{H}_{NOM}$, seems to retain the advantages of both the open-loop and the closed-loop control laws and is believed to be superior to the current control laws. This mixed-mode control law is further described in Section 5.4.

Another mixed-mode law that has a simpler implementation can be derived from the original "simple cross product law," i.e.,

$$\vec{T}_D = \vec{T}_M(t) + \Delta\vec{T}(t) \tag{5-5}$$

where

$$\Delta\vec{T}(t) = K \left[\vec{H}_{NOM}(t) - \vec{H}(t)\right]/\Delta t \tag{5-6}$$

and

$$\vec{T}_M(t) = \tilde{B}(t)\ WW^T\ \tilde{B}^T(t)\ \vec{P} \tag{5-7}$$

_____

[1]It is shown from the simulation results that, in the case of ST, the optimal value for Δt is about 200 seconds. The updating frequency--i.e., the frequency at which $\vec{T}_D$ is calculated--is independent of Δt. To keep the advantages of the closed-loop aspects of this technique, the updating frequency can remain at 50 seconds.

The costate vector, $\vec{P}$, and the representation of $\vec{H}_{NOM}(t)$ are both precomputed.

5.3 DISCUSSION OF CURRENT CONTROL LAWS

Table 5-3 summarizes the equations used for the original and
current control laws implemented for ST. Two alternative
control laws (numbers 3 and 5) are also included in the
table for comparison. Control law 1 is the original CP law,
which is a closed-loop control law that minimizes the dif-
ference between the magnetic torque $\vec{T}_M$ and the desired
torque $\vec{T}_D$. In the determination of $\vec{T}_D$, the original CP
law ignores the gravity-gradient torque, $\vec{T}_{GG}$, and replaces
the system momentum $\vec{H}_T$ by $\vec{H}_{RW}$, which is inefficient for
attitude maneuvers. Control law 2 is the current CP law
implemented onboard ST, which is a modified version of the
original CP law. The current CP law is a closed-loop con-
trol law that minimizes the reaction wheel speed. It im-
proves the determination of $\vec{T}_D$ by including the
gravity-gradient torque, $\vec{T}_{GG}$, and replacing $\vec{H}_{RW}$ by $\vec{H}_T$
to cover the case of maneuvers. It also provides a center
speed control loop to constantly update the value of $\vec{H}_B$
instead of fixing $\vec{H}_B$ at a predetermined value. Control
law 3 is an alternative closed-loop control law that is sim-
ilar to the current CP law except that it minimizes the
energy consumption while keeping the projection of $\vec{T}_M$ on
$\vec{T}_D$ as large as possible. Control law 4 is the current MF
law implemented onboard ST, which is a modified open-loop
control law that minimizes the energy. In control law 4, a
nominal momentum profile $\vec{H}_{NOM}$ is computed for each of the
inertial attitudes using a half-orbit as the desaturation
period. This $\vec{H}_{NOM}$ is then used in the determination of
$\vec{H}_D$ when a shorter desaturation period (600 seconds) and
updating frequency (200 seconds) are used. As discussed in
Section 5.2.2, the purpose of this modification is to reduce
the error made in an open-loop control law in case unde-
tected failure conditions exist. Control law 5 is an al-
ternative open-loop control law that is similar to the

Table 5-3. Summary of Control Law Equations

CONTROL LAW ID	DESCRIPTION	DESIRED TORQUE $\vec{T}_D$	DESIRED MOMENTUM $\vec{H}_D = \int_{t_i}^{t_f} \vec{T}_D$	COSTATE VECTOR $\vec{P}$	SYSTEM MAGNETIC DIPOLE MOMENT $\vec{\mu}_M$	MAGNETIC TORQUE $\vec{T}_M = \vec{\mu}_M \times B$	COMMANDED MAGNETIC DIPOLE MOMENT $\vec{\mu}_T = M^T(MM^T)^{-1}\vec{\mu}_M$
1	ORIGINAL CP LAW	$-K_M(\vec{H}_{RW}+\vec{H}_B)$	NOT APPLICABLE	$(\tilde{B}^T\tilde{B})^{-1}\vec{T}_D$	$\tilde{B}\vec{P}$	$\tilde{B}\tilde{B}^T\vec{P}$	$M^T(MM^T)^{-1}\tilde{B}\vec{P}$
2[a]	CURRENT CP LAW	$-K_M(\vec{H}_T+\vec{H}_B)-\vec{T}_{GG}$	NOT APPLICABLE	$(\tilde{B}^T WW^T \tilde{B})^{-1}\vec{T}_D$	$WW^T\tilde{B}\vec{P}$	$\tilde{B}(WW^T\tilde{B})\vec{P}$	$M^T(MM^T)^{-1}WW^T\tilde{B}\vec{P}$
3	ALTERNATIVE CLOSED-LOOP CONTROL LAW	$-K_M(\vec{H}_T+\vec{H}_B)-\vec{T}_{GG}$	NOT APPLICABLE	$(\tilde{B}^T MM^T \tilde{B})^{-1}\vec{T}_D$	$MM^T\tilde{B}\vec{P}$	$\tilde{B}MM^T\tilde{B}\vec{P}$	$M^T\tilde{B}\vec{P}$
4[a]	CURRENT ME LAW	$\dot{\vec{H}}_{RW}-\vec{T}_{GG}$	$\vec{H}_{NOM}(t_f)-\vec{H}_{RW}(t_i)-\int_{t_i}^{t_f}\vec{T}_{GG}$	$\left[\int_{t_i}^{t_f}\tilde{B}^T MM^T\tilde{B}\right]^{-1}\vec{H}_D$	$MM^T\tilde{B}\vec{P}$	$\tilde{B}MM^T\tilde{B}\vec{P}$	$M^T\tilde{B}\vec{P}$
5	ALTERNATIVE OPEN-LOOP CONTROL LAW	$\dot{\vec{H}}_{RW}-\vec{T}_{GG}$	$\vec{H}_{NOM}(t_f)-\vec{H}_{RW}(t_i)-\int_{t_i}^{t_f}\vec{T}_{GG}$	$\left[\int_{t_i}^{t_f}\tilde{B}^T WW^T\tilde{B}\right]^{-1}\vec{H}_D$	$WW^T\tilde{B}\vec{P}$	$\tilde{B}(WW^T\tilde{B})\vec{P}$	$M^T(MM^T)^{-1}WW^T\tilde{B}\vec{P}$

[a] CONTROL LAW CURRENTLY IMPLEMENTED ONBOARD ST.

current ME law except that it minimizes the reaction wheel speed caused by the secular term of $\vec{T}_{GG}$. $\vec{H}_{NOM}$ should also be computed under the same criteria.

Notice that in the determination of $\vec{T}_D$ and $\vec{H}_D$ for the current ME law, the total momentum $\vec{H}_T$ given in Equations (5-1) and (5-2) has been replaced by the reaction wheel momentum $\vec{H}_{RW}$. This is due to the special way the current ME law is implemented (refer to Secton 2.3.2.1), which does not require knowledge of the system momentum during maneuvers. In the case of maneuvers, the normal mode of operation of the current ME law with a 600-second desaturation period and 200-second updating frequency is terminated. It is replaced by a single maneuver desaturation period which includes a lead time before the start of the maneuver and a lag time after the end of the maneuver. Thus, the length of the maneuver desaturation period depends on the lengths of the maneuver and the lead/lag times. In the current onboard implementation, each maneuver has a single lead/lag time that will be determined by the STOCC and uplinked to the spacecraft with the maneuver commands.

The drawbacks of the current ST momentum management implementation are summarized below.

1.   The current CP law is not an ideal control law because of the general problems associated with all the closed-loop control laws (refer to Section 5.2.2). In summary, it does not take advantage of the variations in geometry and therefore does not dump the right amount of momentum at the right time. As a result, a great deal of energy is wasted in changing the direction of the momentum and dumping the momentum generated by the periodic portion of the gravity-gradient torque.

2.   The current ME law uses the energy minimization criterion, which may not be the best choice for ST momentum management. Minimizing the wheel speed may be more important than minimizing the energy. In other words, the ST requirements may be better met if the current ME law is re placed by control law 5 in Table 5-3.

3.   At inertial attitudes, the current ME law uses 600-second desaturations periods with 200-second updating frequencies to reduce the possible error introduced by undetected failure conditions. However, this choice of desaturation period and updating frequency is still not optimal. The updating frequency of the control law can be further improved if the "mixed-mode control law" described in Section 5.2.2 is used; this is a closed-loop control law operated with the precomputed open-loop $\overrightarrow{H}_{NOM}$. Details of this control law are given in Section 5.4.

4.   Another drawback of the current ME law is excessive wheel speed after slew maneuvers, especially under undetected failure conditions (see Section 4). This problem with maneuvers is caused by the special way the maneuvers are handled in the current ME law. Depending on the length and geometry of the maneuver and the length of the lead/lag time used, the maneuver desaturation period may be too short to provide enough geometrical variation, while on the other hand, it may also be too long to recover an error caused by undetected failure conditions because the magnetic dipole command is not updated throughout the maneuver desaturation period. It is very difficult to define the maneuver desaturation period so that both requirements can be met at the same time.

Because of the drawbacks with the current implementation, alternative techniques are suggested for both inertial and maneuver cases to improve the current situation. These

techniques require minor modifications to the onboard imple-
mentation and are described in the following subsection.

5.4 ALTERNATIVE TECHNIQUES

Because of the problems associated with the current control laws as discussed in Section 5.3, a new technique called the "mixed-mode MWS law" is suggested to replace the current ME law. This mixed-mode MWS[1] law has already been introduced in Section 5.2.2 and is given in more detail in this subsection. In addition, to resolve the current problems with maneuvers, a technique of implementing the mixed-mode MWS law during maneuvers also is presented.

5.4.1 ALTERNATIVE TECHNIQUE AT INERTIAL ATTITUDES

The mixed-mode MWS law is a closed-loop minimum wheel speed control law operated with an open-loop $\vec{H}_{NOM}$. For the case of inertial attitude, $\vec{H}_{NOM}$ is obtained as in Figure 3-1 except that in the computations of $\vec{P}$ and $\vec{T}_M$, the operator $MM^T\vec{B}$ is replaced by $WW^T\vec{B}$. Once $\vec{H}_{NOM}$ is obtained, a closed-loop MWS law will be used onboard that computes $\vec{T}_D$ through Equation (5-4), with $\vec{H}_T(t)$ replaced by $\vec{H}_{RW}(t)$. This technique at inertial attitudes is summarized in Figure 5-3. The advantages of this new technique over the current control laws are given below.

5.4.1.1 Advantages Over the Current CP Law

The mixed-mode MWS law is better than the current CP law because it computes the desired torque based on the nominal momentum profile precomputed using an open-loop control law

with half-orbit desaturation period. The desired torque so determined has the following advantages:

1. It takes advantage of future geometrical variations so that the proper amount of momentum will be dumped at the proper time.

---

[1]The MWS criterion is used for historical reasons in ST momentum management. The ME criterion could also be used in other applications.
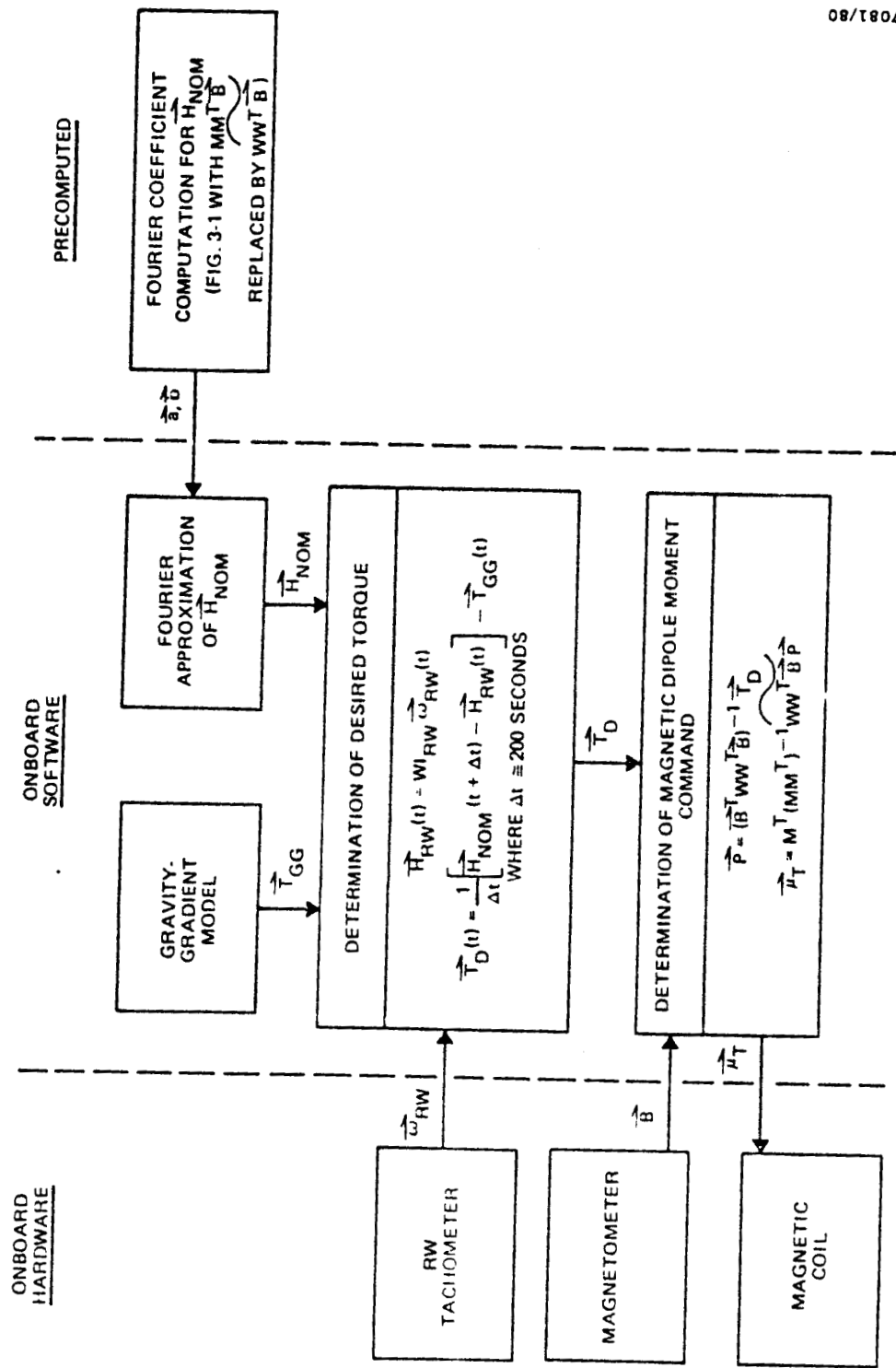
Figure 5-3. Baseline Diagram of Mixed-Mode MWS Control Law at Inertial Attitudes

PRECOMPUTED

FOURIER COEFFICIENT COMPUTATION FOR $\vec{H}_{NOM}$ (FIG. 3-1 WITH $MM^T \vec{B}$ REPLACED BY $WW^T \vec{B}$)

$\vec{a}, \vec{b}$

7081/80

ONBOARD SOFTWARE

FOURIER APPROXIMATION OF $\vec{H}_{NOM}$

$\vec{H}_{NOM}$

GRAVITY-GRADIENT MODEL

$\vec{T}_{GG}$

DETERMINATION OF DESIRED TORQUE

$\vec{H}_{RW}(t) = WI_{RW} \vec{\omega}_{RW}(t)$

$\vec{T}_D(t) = \frac{1}{\Delta t}\left[\vec{H}_{NOM}(t+\Delta t) - \vec{H}_{RW}(t)\right] - \vec{T}_{GG}(t)$

WHERE $\Delta t \cong 200$ SECONDS

$\vec{T}_D$

DETERMINATION OF MAGNETIC DIPOLE MOMENT COMMAND

$\vec{P} = (\vec{B}^T WW^T \vec{B})^{-1} \vec{T}_D$

$\vec{\mu}_T = M^T(MM^T)^{-1} WW^T \vec{B} \vec{P}$

$\vec{\mu}_T$

ONBOARD HARDWARE

RW TACHOMETER

$\vec{\omega}_{RW}$

MAGNETOMETER

$\vec{B}$

MAGNETIC COIL

5-22

2. Only the nonperiodic portion of the gravity-
    gradient momentum will be dumped by the magnetic
    torquers.

3. The desired torque is always nearly perpendicular
    to the geomagnetic field so that very little energy
    will be wasted in changing the direction rather
    than reducing the magnitude of the momentum.

4. The reaction wheel center speed control loop is no
    longer needed because the targeting momentum $\vec{H}_{NOM}$
    automatically keeps the reaction wheel center speed
    at zero. This greatly simplifies the onboard com-
    putation, as can be seen by comparing Figure 5-3
    with Figure 2-3.

5.4.1.2 Advantages Over the Current ME Law

The mixed-mode MWS control law has the following advantages
over the current ME law:

1. It reduces the updating frequency of the magnetic
    coil commands from 200 seconds to approximately
    50 seconds. This will reduce the deviation between
    the actual and the predicted results when unde-
    tected failure conditions exist.

2. It uses the MWS instead of the ME minimization cri-
    terion, which may be advantageous if large wheel
    speeds should be avoided.

3. There is no need of defining a desaturation period
    onboard. This eliminates the possibility of having
    a near-singularity condition in computing the co-
    state vector $\vec{P}$.

4. The required onboard computation for inertial point-
    ing is much simplified because it does not require
    the predicted geomagnetic field computation, and no

integration is involved. This can be seen by comparing Figure 5-3 with Figure 2-6.

5.4.2 ALTERNATIVE TECHNIQUE FOR MANEUVERS

The mixed-mode MWS law can be slightly modified to cover the case of maneuvers so that the current drawback with maneuvers (number 4 given in Section 5.3) can be resolved. Two fundamental factors complicate the situation during maneuvers: (1) the spacecraft body coordinate is no longer fixed in inertial space and (2) the nominal momentum profile $\vec{H}_{NOM}$ can no longer be represented by a simple first-order Fourier expansion. To overcome the first complication, a command generator (currently implemented onboard) is required to compute $\Gamma_{t,t'}$, the coordinate transformation between the body coordinates at two different times. To overcome the second complication, instead of storing the Fourier coefficients, the costate vector P that is precomputed using a half-orbit desaturation period can be stored onboard for computing $\vec{H}_{NOM}$. Since P remains constant for the entire desaturation period, the value of $\vec{H}_{NOM}$ at any time within the desaturation period can always be computed from P using the equation for $\vec{T}_M$ and integrating Equation (2-4) once P is obtained. The implementation of the mixed-mode MWS control law for maneuvers is shown in Figure 5-4. With this implementation, in addition to the Fourier coefficients, computed for each of the inertial attitudes, a costate vector for each of the maneuvers also is required. The maneuver desaturation period is chosen to cover the period from a half-orbit before the end of the maneuver to the end of the maneuver to ensure large geometrical variations.[1] This eliminates the necessity of

---

[1] While a shorter period may be desirable, long desaturation periods are not of concern because the mixed-mode control law updates commanded torques frequently, eliminating problems due to failure conditions.

Figure 5-4. Baseline Diagram of Mixed-Mode MWS Control Law for Maneuvers

determining the lead/lag time for each of the maneuvers. In case the start time of the maneuver desaturation period so determined falls within another maneuver, then the end time of the maneuver should be used instead. This start time of the maneuver desaturation period should also be kept onboard for each of the maneuvers in addition to the costate vector $\vec{P}$. The control law given in Figure 5-3 will be used onboard at an inertial attitude until the start time of a maneuver desaturation period is reached. Then the control law will be switched to that given in Figure 5-4 until the end of the maneuver.

In Figure 5-4, the times in the superscripts indicate the times associated with the body coordinate systems in which the quantities are represented, while the times in the parentheses give the times at which the quantities are evaluated or measured. When there is no superscript, the two times will be the same; that is, the instantaneous body coordinate system is used. Figure 5-4 is similar to Figure 5-3 except that more onboard computation is required to compute the nominal momentum profile and the coordinate transformations. Actually the capability of computing the coordinate transformation during maneuvers already exists in the current implementation onboard ST. It is done by a simplified command generator that is turned on whenever the maneuver exceeds 10 degrees (Reference 5-1). Thus, no additional computational module is required onboard for this purpose. The computation of $\vec{H}_{NOM}$ at a given time can be done by propagating $\vec{H}_{NOM}$ from a previous time as shown in Figure 5-4, which involves very simple and straightforward processing.

The mixed-mode MWS technique for maneuvers given in Figure 5-4 overcomes current drawbacks with maneuvers because it updates the magnetic dipole commands at a closed-loop frequency throughout the maneuvers so that much better

control over the reaction wheel speed is expected after each maneuver, especially when undetected failure conditions exist.

In summary, with minor modifications to the current control laws implemented for ST, the alternative techniques shown in Figures 5-3 and 5-4 for the inertial and maneuver cases, respectively, seem to provide many advantages over the current control laws. Thus, these new techniques should be seriously considered as possible replacements for the current control laws. Simulation results are shown in Section 7 to compare the performance of this mixed-mode control law with the performance of the current control laws.

REFERENCE

5-1. Lockheed Missiles and Space Company, LMSC 4172682, ST
PCS Flight Software Algorithms, R. H. Jones, W. F.
Wright, and W. H. Whittier, October 1979

SECTION 6 – MATHEMATICAL MODEL ACCURACIES

This section discusses published accuracy requirements for the mathematical models used in the implementation of the CP and ME laws, which were presented in Sections 2 and 3.

6.1 MATHEMATICAL MODELS

The onboard implementation of the CP and ME control laws is summarized in Figures 2-3 and 2-6. The ultimate output from either law is the magnetic dipole moment command given by

$$\vec{\mu}_T = M^T \left(MM^T\right)^{-1} \frac{\vec{B'} \times \vec{T}_D}{\vec{B'} \cdot \vec{B}} \tag{6-1}$$

for the CP law and by

$$\vec{\mu}_T = \vec{M}^T \vec{B}_c \times \vec{P} \tag{6-2}$$

for the ME law. M is the magnetic coil mounting matrix. $\vec{B}$ is the geomagnetic field measured by two redundant three-axis magnetometers and $\vec{B}_c$ is that calculated from the onboard geomagnetic field model.[1]

Onboard implementation of the CP law requires determination of the desired torque, $\vec{T}_D$, which is calculated from

$$\vec{T}_D = - \vec{T}_{GG} - K_M \left(\vec{H}_T + K_P \vec{H}_{CSD} + K_{\Sigma} \vec{\Sigma}\right) \tag{6-3}$$

---

[1] Note that in Section 6 the subscript "c" is used to denote calculated values.

Parameters in the second term on the right of Equation (6-3) are determined from RW tachometer and RGA data. The gravity-gradient torque, $\vec{T}_{GG}$, is calculated from

$$\vec{T}_{GG} = 3\Omega_o^2 \left[\hat{R}_V \times (I\hat{R}_V) \right]$$

where I is the ST inertia matrix, Ω_o is the vehicle orbital rate, and $\hat{R}_V$ is the unit ST position vector in the spacecraft body-fixed coordinate system.

The costate vector, $\vec{P}$, required for implementation of the ME law at inertial attitudes is given by

$$\vec{P} = \left[\int_{t_o}^{t_f} \tilde{B}_c MM^T \tilde{B}_c^T \, dt \right]^{-1} \vec{H}_D \qquad (6-5)$$

where

$$\vec{H}_D = \vec{H}_{NOM}(t_f) - H_{RW}(t_o) - \int_{t_o}^{t_f} \vec{T}_{GG} \, dt \qquad (6-6)$$

New parameters introduced in Equations (6-5) and (6-6) are defined as follows:

- $t_f = t_o + 600$ seconds and t_o is incremented in steps of 200 seconds.

- $\tilde{B}_c$ is the dyadic representation of the magnetic field (Equation (2-30)) calculated from the onboard geomagnetic field model.

- $\vec{H}_{NOM}$ is the approximation of the nominal momentum calculated from Fourier coefficients provided by the STOCC.

- $\vec{H}_{RW}$ is the RW system momentum derived from RW tachometer measurements.

The computation of the Fourier coefficients of the nominal momentum profile by the STOCC is summarized in Figure 3-1. The Fourier coefficients are computed from the equations

$$\vec{a} = \frac{2}{T} \int_{T_o}^{T_o+T} \vec{H}_{NOM}(t) \cos\left(\frac{2\pi}{T}t\right) dt$$

(6-7)

$$\vec{b} = \frac{2}{T} \int_{T_o}^{T_o+T} \vec{H}_{NOM}(t) \sin\left(\frac{2\pi}{T}t\right) dt$$

The nominal momentum profile is given by

$$\vec{H}_{NOM}\left(t_i\right) = \int_{T_o}^{t_i} \left(\vec{T}_M(t) + \vec{T}_{GG}(t)\right) dt$$

(6-8)

where

$$\vec{T}_M\left(t\right) = \vec{B}_c\left(t\right) \times \left[MM^T\left(\vec{B}_c\left(t\right) \times \vec{P}\right)\right]$$

(6-9)

$$\vec{P} = \left[\int_{T_o}^{T_o+T} \tilde{B}_c MM^T \tilde{B}_c^T dt\right]^{-1} \left[-\int_{T_o}^{T_o+T} \vec{T}_{GG} dt\right]$$

(6-10)

$\vec{B}_c$ and $\tilde{B}_c$ are calculated from a geomagnetic field model, and $\vec{T}_{GG}$ is calculated from Equation (6-4) using the ST ephemeris available to the STOCC.

T_o is the time at the end of the last slew maneuver and T is the half-orbit period. Complete details of numerical integrations used in Equations (6-7) through (6-10) are given in Section 3.

6.2 ACCURACY REQUIREMENTS·AND ESTIMATES

The accuracies of the calculations reviewed in Section 6.1 depend on the accuracies of sensor observations, alignment estimates of sensors and magnetic coils, and mathematical models, including the integration techniques used. Estimates of the magnetic coil mounting matrix, M, and the alignment matrices for the RWs and RGAs can be refined from an evaluation of the in-flight performance of the system. Biases in the measurement of $\vec{B}$ can also be determined from postlaunch analysis. Requirements to estimate alignments and biases of magnetic coils, magnetometers, and other sensors and corresponding accuracy requirements for such determinations have not yet been published in Space Telescope Mission Operations Requirements (Reference 6-1). The remainder of this section discusses published accuracy requirements and estimates for the mathematical models.

The accuracy of calculations performed by the STOCC is discussed by Wernli in Reference 6-2. Two accuracy requirements stated in that document are

1.   The accuracy of the magnetic field model should be such that the peak vector error is less than 10 percent.

2.   The error in $\vec{H}_{NOM}$ referenced to the peak value of $|H_{NOM}|$ should not exceed 2 percent.

The latter requirement is repeated in Reference 6-3.

Wernli states that a six-dipole representation of the geomagnetic field can be used to fulfill requirements for both STOCC and onboard processing. The peak vector error in this representation is approximately 6 percent, with a root-mean-square error of about 2 percent. Wernli also states that a

30-kilometer position error in the ST ephemeris results in a gravity-gradient torque error of about 1 percent and a geomagnetic field error of about 2 percent. Presumably the geomagnetic field error due to ST position error is in addition to any error in the magnetic field model. The effects of errors in $\vec{B}_c$ and $\vec{T}_{GG}$ on the accuracy of $\vec{H}_{NOM}$ are not discussed in Reference 6-2. The results of an analysis of integration techniques were presented, however. To achieve an accuracy of 2 percent in $\vec{H}_{NOM}$, Wernli recommends a maximum step size of 600 seconds when a fourth-order Runge-Kutta integration technique is used.

Specific requirements for the ephemeris accuracies necessary to perform mission planning and scheduling are given in Table 3-1 of Reference 6-1. In this table the tentative accuracy requirement for the geomagnetic field strength (used for purposes of momentum management) is listed as 4 percent (TBD)[1]. The computed in-track ephemeris accuracy needed to realize this requirement is listed as 60 kilometers (TBD). It is further stated that orbit determinations are required 2-1/2 (TBD) weeks prior to the observation. The relation in Reference 6-1 between ephemeris and magnetic field errors (60 kilometers versus 4 percent) is consistent with the statement in Reference 6-2 that a 30-kilometer position error causes a 2-percent error in the magnetic field determination. Neither reference defines the type of error (e.g., peak or root-mean-square) that is used. Therefore, it is unclear how to combine the magnetic field error due to ephemeris inaccuracy with error due to the magnetic field model. Note that the 4-percent error due to ephemeris inaccuracy plus the 6-percent peak error (Reference 6-2) due to model inaccuracy equals the 10-percent accuracy requirement for $\vec{B}_c$ specified in Reference 6-2.

---

[1] TBD, "To Be Determined," is defined in Reference 6-1 as follows: "To the present level of understanding, the subject identified by TBD is: a.) within scope of existing contracts or within the Project planning baseline, but the subject needs better definition, or b.) at present, there are no data available regarding the item which would permit review and assessment."

In addition to the ephemeris required for mission planning and scheduling, ephemeris information for onboard processing must be supplied. Reference 6-3 specifies that the state vector used onboard for the calculation of the ST orbital position "... shall be update(d) at a frequency of 72 hours or less, and shall be specified with precision sufficient to maintain a 25 Km in-track accuracy over the 72 hours." The state vector contains Keplerian orbital elements from which the position is calculated using the equivalent of the standard expansion in terms of the eccentricity and mean anomaly (Reference 6-4). The effects of atmospheric drag are incorporated in the state vector itself (Reference 6-5).

Unofficial information (Reference 6-5) indicates that the accuracy requirement for the ST ephemerides may be relaxed to 120 kilometers for both ground and onboard processing with update frequencies of 8 to 10 days for the ground processing and 3 days for onboard.

A summary of available mathmetical model accuracies and requirements is provided in Table 6-1. The first column of Table 6-1 gives the parameter. The second column gives specified accuracy requirements, when available. The ST position requirement is the one stated in Reference 6-1, which is necessary to maintain the desired magnetic field accuracy. The requirement for $\vec{B}_c$ is taken from Reference 6-2 and appears to include allowance for errors from both the model and the ST position. The third and fourth columns give the estimated accuracies of $\vec{T}_{GG}$ and $\vec{B}_c$ for ST position accuracies of 30 kilometers and 120 kilometers, respectively. Errors in $\vec{B}_c$ due to the model and ST position errors are stated, but no attempt is made to combine these errors. The accuracy of $\vec{H}_{NOM}$ as a function of $\vec{T}_{GG}$ and $\vec{B}_c$ is unavailable.

This review of available documents reveals several deficiencies in the accuracy requirements for ST momentum management. These include the following:

- Requirements to estimate alignments and biases of magnetic coils, magnetometers, and other sensors and corresponding

Table 6-1. Mathematical Model Accuracies
and Requirements

Parameter	Requirement	Accuracy Estimates	
ST position	60 kilometers[1]	30 kilometers	120 kilometers
$\vec{T}_{GG}$	–	1 percent	4 percent
$\vec{B}_c$	10 percent[2]	(6 percent + 2 percent)[3]	(6 percent + 8 percent)[3]
$\vec{H}_{NOM}$	2 percent	–	–

---

[1] Reference 6-1.

[2] Reference 6-2.

[3] Includes the peak vector error due to the geomagnetic field model and the error due to ephemeris inaccuracy.

accuracy requirements for such determinations have not yet been published in <u>Space Telescope Mission Operations Requirements</u> (Reference 6-1).

- No accuracy requirement for the calculation of $\vec{T}_{GG}$ is available in the documents reviewed.

- The accuracy requirement for the calculated geomagnetic field in Reference 6-1 appears not to include allowance for the errors due to the field model.

- No analysis of the combination of geomagnetic field errors due to field models and ST ephemerides is available in the documents reviewed.

- No analysis of the effect on $\vec{H}_{NOM}$ of errors in the ST ephemeris, $\vec{T}_{GG}$, and $\vec{B}_c$ is available in the documents reviewed.

It is recommended that investigation of these deficiencies be initiated to establish confidence in the ability of the ST momentum management techniques to perform their required functions.

REFERENCES

6-1. Lockheed Missiles and Space Company, LMSC 4171847D, ST Mission Operations Requirements, OP-01, Volume III, March 1980

6-2. --, SE EM No. PCS-205, Momentum Management Computations Performed by STOCC, A. Wernli, July 1978

6-3. --, LMSC 4171874B, ST Mission Operations Requirements (Appendix A – Ground Computational Support Requirements), October 1979

6-4. --, LMSC 4172682, ST PCS Flight Software Algorithms, R. H. Jones, W. F. Wright, and W. H. Whittier, October 1979

6-5. J. Hennessy (GSFC), private communication, 1980